A new method for measuring the scattering coefficient and the diffusion coefficient of panels

Angelo Farina

Dipartimento di Ingegneria Industriale, Università di Parma,
Via delle Scienze - 43100 PARMA, ITALY - tel. +39 0521 905701 - fax +39 0521 905705
E-MAIL: farina@pcfarina.eng.unipr.it - HTTP://pcfarina.eng.unipr.it

Abstract

The sound scattering properties of diffusing panels are actually very difficult to measure and to predict. In this paper the Wave Field Synthesis approach is employed for the experimental measurement of the scattering coefficient. The results are in good agreement with the numerical simulations made possible by some recent improvements to the Pyramid Tracing algorithm, which takes into account separately the scattering of sound from the edges of finite-size surfaces, and the surface scattering coefficient.

1. Introduction

Recently, both AES and ISO activated working groups with the goal of standardizing measurement procedures for the characterization by a single number of the behaviour of diffusing panels.

AES formed the SC-04-02 standard committee, with the goal of providing a standard for the definition and measurement of the diffusion coefficient, which is a measure of the spatial uniformity of the sound globally reflected by an object [1,2]. In the AES approach, no distinction is attempted between specular reflection or diffuse reflection, nor the edge scattering is explicitly addressed: everything which comes back from a finite-size object is taken into account. A statistical descriptor is evaluated based on the acoustic intensities measured on N points equally spaced over an hemispherical surface, centred in the midpoint of the diffusing object:

$$d = \frac{\left(\sum_j I_j\right)^2 - \sum_j \left(I_j^2\right)}{(N-1)\cdot \sum_j \left(I_j^2\right)} \qquad (1)$$

The value of the diffusion coefficient approaches zero when the reflected sound is concentrated over a little number of measurement points, and approaches 1 when the reflected intensity is uniform on the hemisphere.

ISO formed the working group ISO/TC43/SC2/WG25 with the goal of providing a standard for the definition and measurement of the scattering coefficient, defined as the ratio between the sound energy reflected diffusely by an infinite surface and the total reflected energy (diffuse + specular):

$$s = 1 - \frac{E_{spec}}{E_{total}} \qquad (2)$$

Thus, the ISO approach yields a value compatible with the requirements of many room acoustics computer programs, at the price of a measurement procedure which is more delicate and requires an expensive laboratory setup [3].

It is evident that the scattering coefficient is generally a quantity very different from the diffusion coefficient.

In this paper, moving from the Wave Field Synthesis approach developed at the Tech. University of Delft [4,5,6], it is shown how it is possible to characterise completely the scattering properties of a generic, finite-size object by a large number of impulse response measurements taken moving the microphone at small steps along a straight line.

From this characterisation, by best matching with the theoretical behaviour of an absorbing/diffusing object, and after separation of the edge diffraction effect, it is possible to obtain a surface scattering coefficient compatible with the ISO definition. Simultaneously it is possible to derive also the AES diffusion coefficient.

In this work it is also described how a congruent scattering treatment was implemented inside a room acoustic numerical model, based on the Pyramid Tracing approach. The modified algorithm does not suffer of increased computation time, because it was possible to maintain a single geometrical tracing, covering simultaneously 10 octave bands.

2. Theoretical relationship between ISO scattering coeff. and AES diffusion coeff.

The definitions of the scattering and diffusion coefficients are substantially consistent for the extremes of the scale: a flat, very large, polished panel for which is s=0 will be probably measured with very little values of d, and instead an highly diffusing surface, with an almost uniform polar pattern of the reflected intensity (and no specular reflection) will give unitary values for both coefficients.

But in intermediate cases, the qualitative nature of the diffusion coefficient and the quantitative nature of the scattering coefficient cause significantly different values. This can be verified easily in the following two cases.

Consider first the case of a panel, which scatters the sound in all directions, but with pronounced lobes modulating the radiation of the diffused energy between a constant maximum and a much lower minimum. In this case, the amount of energy which goes in the "specular" direction is negligible, and thus the scattering coefficient s approaches 1.

Fig. 1 shows the polar pattern of the reflected energy, in the case of sound that is impinging on the panel along the normal to its surface. Almost no energy is reflected back in the specular direction, the whole reflected energy is scattered around. But the scattered intensity is not spatially uniform, and this reduces significantly the value of the diffusion uniformity coefficient (d =0.5) compared with the theoretical value of 1.

Consider then the case of a panel, which exhibit an evident specular behaviour, so that 70% of the reflected energy goes in the specular direction corresponding with the Snell's law. But the other 30% of the reflected energy is spread uniformly in all directions (uniform scattering, not Lambert scattering). In this case, by definition, s is 0.3, but instead the value of d depends on the geometry of the measurement set-up. In fact, the ratio between the distance of the panel and the sound source (r_1), and the distance of the panel and the microphones (r_2) influences the ratio between the specular intensity and the diffused intensity, and so the value of d can assume almost any value.

This was checked by numerical simulation of a test case, in which an omni directional point source is located at a distance r_1 = 10 m, in front of the panel (θ=90°), whilst a semicircular array of 37 microphones (spaced 5°) is surrounding the diffusing panel, at a

distance r_2=5m, as shown in fig. 2. The size of the panel is assumed to be 1m x 1m (S_{panel} = 1 m^2) and thus it intercepts a fraction $S_{panel}/(4\pi r_1^2)$ of the total radiated sound power W. The absorption coefficient is assumed zero, and no edge effect was considered. The specularly-reflected sound intensity received by the three microphones in the specular zone (the central one and the two adjacent) is:

$$I_{spec} = \frac{W \cdot (1-s)}{4 \cdot \pi \cdot (r_1 + r_2)^2} \tag{3}$$

Instead, the diffuse sound intensity received by all the microphones (including the three central ones, where it sums to the above specular intensity) is:

$$I_{diff} = W_{inc} \cdot \frac{s}{2 \cdot \pi \cdot r_2^2} = \frac{W \cdot S_{panel}}{4 \cdot \pi \cdot r_1^2} \cdot \frac{s}{2 \cdot \pi \cdot r_2^2} \tag{4}$$

Fig. 3 reports the polar pattern of the reflected intensity, resulting from the above calculations, when the scattering coefficient s is 0.3. From such a distribution of sound intensities, the diffusion coefficient d can be computed following its definition: it resulted equal to 0.061426, which is quite different from s. This demonstrates that the two quantities s and d are inherently different, and they must not be confused: in particular, it is conceptually wrong to introduce the values of the diffusion coefficient in most room acoustics computer programs, which instead are usually expecting for the values of the scattering coefficient.

The last point to discuss is the "scattering model" which is assumed to represent an ideally diffusing surface. Two models are widely employed in different sciences, regarding other types of radiation: the uniform scattering and the Lambert scattering. The first model is the simplest one, as it assumes that the diffuse intensity reflected by the surface is constant in any direction; the second one is instead related to the Lambert's law, initially enunciated for the thermal radiation from a "black body", which states that the intensity of the diffuse radiation (in that case it is not reflected, it is generated by the black body, which by definition does not reflect anything) varies with the cosine of the angle between the direction of observation and the normal to the surface in the observation point.

Although some room acoustics program are employing the Lambert model for redistributing the diffuse energy after a reflection [7,8], in this work it will be assumed that the ideal behaviour of a perfectly diffusing surface corresponds to the uniform scattering model. This assumption is caused by two facts: first, the AES diffusion coefficient is based on a statistic over the reflected intensity, and thus it requires an uniform intensity for producing its maximum value; second, the numerical simulations conducted with the uniform scattering model revealed to match with the experimental results better, on average, than those conducted with the Lambert model.

3. The Wave Field Synthesis (Analysis) approach

Wave Field Synthesis was initially developed at the Tech.University of Delft as a technique for producing synthetic sound fields, thanks to linear arrays of loudspeakers [4]. More recently, the technique was folded back to the analysis of complex sound fields, being renamed Wave Field Analysis [5]. In this second application, a large number of impulse responses are measured with a single microphone, repeatedly placed in subsequent positions along a straight line, with constant spacing.

After the impulse responses are measured, an image is formed plotting the magnitude of the signal along a vertical line for each microphone in terms of darkness of the pixels. This graphing technique is common in other fields, such as underwater acoustics or medical imaging. Important information can then be obtained applying to such images proper data processing

techniques, the most simple being windowing and filtering, going up to deformations and synthetic focusing.

In the case of a diffusing panel inserted in a flat surface, this technique evidences the scattered wavefronts from the specularly reflected one, as the first has more curvature than the latter [6]. In principle, this different curvature could be used for separating the two reflected sound fields (specular and diffused), and this would enable the direct computation of the ISO scattering coefficient.

So it was decided to employ a data acquisition technique based on the WFS approach, with a microphone moving along a straight line instead of along a hemi circumference. As it will be explained in the following paragraphs, this made it possible to obtain a better understanding of the reflected sound field than what can be seen by energetic polar plots.

4. Experimental apparatus

A low-cost experimental setup was employed for this work. The experiment was conducted in a large, untreated room: the elimination of unwanted reflections was obtained by time windowing of the measured impulse responses.

The geometry of the testing facility is schematically represented in fig. 4.

A single, wide-band loudspeaker was mounted flush on the floor, in which a proper niche was created. The diffusing panel was suspended just above it, at an height z_c of 3.65 m.

A Soundfield pressure/velocity microphone was moved along a line, at an height z_r over the floor of 1.98 m, passing under the diffusing panel, thanks to a light carriage and a rotating board which acted as drum, over which a cable was folding pulling the carriage. A rail embedded in the floor ensured linear movement of the microphone. The advancement step was 27.91 mm, and 255 microphone positions were measured.

The impulse response measurements were conducted with a PC equipped with an Echo Layla board (capable of simultaneous acquisition of up to 8 channels, at 20 bit, 48 kHz), directly interfaced with the rotating board. The software employed for the measurements was Aurora 3.0 [9], running under CoolEditPro v. 1.2. A Cool Edit macro ensured automatic, unattended operation (the whole measurement procedure was lasting more than three hours).

Each impulse response measurement was constituted of 16 repetitions of the MLS-16A signal (Maximum Length Sequence of order 16). The deconvolution was based on the synchronous average of the latter 15 sequences, as the first one served to bring the system in steady state.

Fig. 5, 6, 7, and 8 show the overall setup, the loudspeaker, the microphone, the rotating board and the suspended panel. As shown, it was attempted to reduce the unwanted reflections from the carriage by covering it with a thick coat of sound absorbing material (which gained it the surname of “sheep”).

Thanks to the employ of a Soundfield MKV microphone, in each microphone position 4 impulse responses were measured simultaneously, coming from the 4 B-Format output connectors of the microphone. The first channel is the omni directional pressure (W), and the other three channels are the Cartesian components of the particle velocity (XYZ). This makes it possible, in principle, to measure the three-dimensional sound intensity; nevertheless, only the pressure channel results were employed for the subsequent computations till now. In the future, a more robust true intensimetric analysis will be conducted on the acquired data, instead of employing the squared pressure in place of the true acoustic intensity.

It was also possible, thanks to the advanced digital signal processing tools included in Aurora, to apply a proper filtering to the measured impulse responses, for “sharpening” the time signature of the loudspeaker. This was possible thanks to the module which computes the Nelson/Kirkeby inverse filter of the loudspeaker response [10], computed selecting the direct wave in the microphone located exactly above the loudspeaker. After the computation of the

inverse filter, it was applied by convolution to the whole sequence of 255 impulse responses, obtaining the deconvolution of the loudspeaker signature to an almost perfect Dirac's delta function.

This process was capable of producing a substantial improvement of the image definition, as it is demonstrated in fig. 9, which compares an original acquisition with the corresponding filtered image. In these images, a grey-scale image is obtained, plotting along vertical columns the logarithmic amplitude of the impulse response, and packing side-by-side the responses of all the 255 microphones. The vertical axis is thus graduated in ms, whilst each horizontal pixel correspond to a single microphone step (27.91 mm).

As the Kirkeby's filtering demonstrated to be very effective, this processing was systematically employed for all the measurements. A further improvement is possible, substituting the MLS signal with the new logarithmic sweep [11]. This method was not employed here because it takes more time for the processing, although it is planned to repeat all the measurements also with this new technique, which already demonstrated to produce better results particularly regarding the peak sharpness and the S/N ratio.

5. Results from the tests on three diffusers

In the following, the results obtained with three different diffusing panels are presented. The first one is a square, flat, smooth panel, made of heavy wood (MDF) and measuring 0.715 x 0.715 m. The second has the same size and is made of the same material, but has evident diffusing properties at medium frequency due to its construction as a sequence of cavities of different depth (it is visible in fig. 8). The third is a hemicylindric surface, also made of smooth wood (marine plywood), measuring 2m x 0.9m. It was measured in two perpendicular directions: the direction of maximum scattering, that is perpendicularly to the cylinder axis, and the orthogonal one (moving the microphone along the cylinder's axis), which exhibits much lower spreading of the reflected sound.

Fig. 10 shows the three WFS representations of the measurement on these three panels, after the Kirkeby equalization. The response of the hemicylinder along its minimum scattering direction was instead shown in fig. 9.

The next step in processing the experimental results was the separation of the direct sound from the reflected waveform. This was possible employing the WFS theory for computing proper spatial windows, and applying them to the above results, setting to zero all the data points outside these windows.

This process is possible on a simple geometrical basis, as the computation of the travelled distance translates easily in the corresponding time lag over the impulse response of each microphone. The windowing process is demonstrated in fig. 11. The experimental response of the curved panel is separated in the direct and reflected parts; the plots of the latter two data-sets have been done with a wider dynamic range (150 dB instead of 100 dB), so that the exact shape of the windows is made evident by the greater depth of the grey scale.

After the windowing, it is possible also to "listen" separately at the direct and reflected sound. The first is always the same for all the measurements, whilst the second reveals the nature of the reflected sound. In fact, the flat panel produces a short impulse (but somewhat smeared for the border effect), the diffusing panels responds with a smooth and long signal, having little impulsive character, and the curved surfaces produces a lower amplitude, but much sharper peak, without any sort of tail. This different behaviour is evident looking at fig. 12, which shows the enlarged portion of the reflected waves for the central microphone.

For the subsequent analysis, the windowed portions were octave-band filtered and the sum of the squared sample values was taken as an estimate of the acoustic intensity of the direct and reflected waves.

6. Evaluation of the AES diffusion coefficient

In its original formulation, the diffusion coefficient has to be evaluated from measurements of the reflected component made with microphones placed along a circular arch, centred in the middle of the panel. In our measurements, instead, the microphones are placed at varying distance from the centre of the panel. So it is necessary to compensate for this varying distance, assuming spherical divergence from the centre of the panel.

With reference to fig. 4, if the distance of the panel from the floor is called z_c, the distance of the microphones from the floor is called z_r, and the current position of each microphone is called x (with x=0 exactly above the loudspeaker), the reflected intensity of each microphone can be corrected as follows:

$$I_{semicircle} = I_{line} \cdot \left(\frac{(z_c - z_r)^2 + x^2}{(z_c - z_r)^2} \right) \tag{5}$$

The angle is then related to the longitudinal position of the microphone with the relationship:

$$\varphi = \arctan\left(\frac{x}{z_c - z_r} \right) + \frac{\pi}{2} \tag{6}$$

With this kind of post processing, the polar pattern of the reflected energy can be constructed for each of the four measured data sets.

Figs. 13, 14, 15, and 16 show the polar patterns at 8 frequencies for the three panels (two data-sets for the hemicylinder, along the maximum and minimum diffusion directions). In fig. 15 it is easy to see how, being the cylindrical diffuser a not-isotropic scatterer, which spreads the sound more in a cylindrical way than in a spherical one, the application of the above equation (6) for spherical correction causes the extreme microphones to be over-corrected, and the polar pattern seems to indicate that more sound is redirected at very low or very high angles than near the specular direction.

From each polar pattern it is quite easy to compute the AES diffusion coefficient, making use of the normalized autocorrelation definition provided in [1,2] and already discussed in this paper (eq. 1). Figs. 17, 18, 19, and 20 show the frequency spectrum of the diffusion (uniformity) coefficient for the three tested panels (as always, two data-sets for the hemicylinder).

It is evident how the diffusion coefficient, being an uniformity estimator, assigns maximum values to the smooth behaviour of the curved panel, although the reflected sound coming from it sounds very “specular”. This must make it clear that the diffusion coefficient does not have any relationship with the temporal structure of the reflected sound and its intrinsic coherence.

7. Estimation of the ISO scattering coefficient

The direct derivation of the scattering coefficient with the method originally suggested by Vorlander and Mommertz [3], and being normalized by ISO, revealed to be quite difficult [12]; thus it was decided to employ here an indirect approach for estimating proper values of the scattering coefficient. An alternative method for obtaining the separation of the scattered and specular reflected intensities will be probably possible working with true intensimetric measurements, hybridising the theory already developed in [13] for the measurement of the absorption coefficient with the Wave Field Synthesis approach, but this will be the goal of future research.

The indirect definition of the scattering coefficient, proposed here as an alternative to the ISO definition, is very pragmatic: we search for the value of the scattering coefficient (and of

the absorption coefficient, at once) which, inserted in a simplified formulation of the reflection (specular, diffuse, and border effect) produces numerical results in optimal agreement with the experimental ones.

In practice, we shall define the scattering coefficient s as the numerical value which, inserted in the simplified formulation given hereafter, makes the numerical simulation of the sound field to be maximally similar to the experimental results.

Like the Sabine's equation, which only describes a very specific case (a diffuse field in a reverberant room), also the following theory only applies to a specific case of very simple reflection/diffusion. In general cases, a room acoustic program will be needed for properly modelling multiple reflection/diffusion paths in complex geometries.

The test case considered here is a free, rectangular panel (dimensions 2· a x 2· b), suspended above a point sound source, and above a row of microphones, as already shown in fig. 4.

At each microphone position, the total diffused energy which comes back from the panel can be computed as:

$$I_{diff} = \int_{y=-b}^{b} \int_{x=-a}^{a} \frac{W \cdot z_c}{4 \cdot \pi \cdot r_1^3} \cdot \frac{(1-\alpha) \cdot s_{loc}}{2 \cdot \pi \cdot r_2^2} \cdot dx \cdot dy \qquad (7)$$

In which s_{loc} is the local value of the scattering coefficient, which can vary due to the increase of the scattering coming near to the edges of the panel. In practice, s_{loc} increases over the normal value of s only starting from a distance x from the border of the panel equal to $\lambda/2$, and it reaches its maximum value (1) at the border itself, following this linear equation:

$$s_{loc} = 1 - (1-s) \cdot \frac{x}{\lambda/2} \qquad (8)$$

Due to the variation of s_{loc}, the analytical computation of the integral contained in eq. (7) is not easy, so it was decided to perform it numerically, inside an Excel spreadsheet. The surface of the panel was divided in 11x11 cells, and from each cell a local contribution to the diffused energy is computed for each microphone.

Furthermore, for the small number of microphones which are within the specular zone, a specular reflected intensity also arrives (apparently being generated at the mirror image source, which is at an height 2· z_c):

$$I_{spec} = \frac{W \cdot (1-\alpha) \cdot (1-s_{loc})}{4 \cdot \pi \cdot \left[(2 \cdot z_c - z_r)^2 + x_r^2 \right]} \qquad (9)$$

After summation of the two intensities, a column of 255 theoretical reflected intensities is obtained, and this is compared with the column containing the experimentally measured values of the reflected intensity.

First of all, the value of the emitted sound power W is adjusted so that the intensity of the direct wave, for the central microphones, assumes exactly the same value as measured. Then the Excel's solver function is employed, for automatically optimising the values of α and s which cause the numerical results to maximally match the experimental data. This process takes some minutes, and after the optimisation is concluded it is possible to compare graphically the results.

Figs. 21, 22, 23 and 24 show the results obtained for the three already described panels (the curved panel is considered twice, both along maximum and minimum diffusion directions).

This table compares the values of the scattering coefficients with the diffusion coefficients, at the frequency of 1 kHz.

Parameter	Flat Panel	Galav2 diffuser	curved panel	curved panel (90°)
α	0	0.03	0.286	0.76
s (ISO)	0.117	0.86	1	0.20
d (AES)	0.35	0.86	0.92	0.52

It can be seen that in some cases the correspondence is very good, but in others the values of s and d are very different. It can be seen also how the curved panel, along its major dimension, behaves as a not-diffusing surface, but it appears to have a much greater absorption coefficient, as the energy is being spread on sides, and thus the specular reflection has lower amplitude than what's expected for a flat surface. This fact already shows that serious errors can arise if the curved panel is modelled as a flat panel with "average" values of α and s.

8. Improvement of the pyramid tracing computer model with inclusion of scattering

The measurement technique previously described produces values of the scattering coefficient δ, which are optimally suited for numerical simulation with geometrical room acoustics programs. Of course, within these programs, a consistent implementation of the scattering treatment needs to be done. Here it is briefly described how the edge and surface scattering phenomena were included in the Pyramid Tracing program developed by the author [14].

The basic principles of Pyramid Tracing are not recalled here, the reader is redirected to available sources [14,15,16]. However, it must be recalled that the algorithm is not hybrid: each pyramid is followed for the whole length of its path, up to a pre-defined time limit (impulse response length), and the intensity is stored for each receiver which happens to be within the pyramid.

This algorithm required only minor modification for taking into account the scattering effects: simply, the energy being propagated within each pyramid is associated with a "running" value of the scattering coefficient $s_{tot}(n)$, which always start from zero (direct sound, when the number of reflections n is equal to zero), and increases reflection after reflection towards one [$s_{tot}(n\rightarrow\infty)=1$]. The meaning of s_{tot} is simply that it separates the total energy in a "diffuse" part and in a "specular" part. As the programs traces simultaneously 10 octave bands, at each frequency an independent value of the energy and of s_{tot} is considered: this way, a single geometrical tracing is required for the whole frequency range.

After each reflection, s_{tot} is recomputed, taking into account the local value of the scattering coefficient s_{loc} in the point hit by the pyramid axis (which can be affected by the edge proximity according to eq. 8):

$$s_{tot}(n+1) = s_{tot}(n) + [1 - s_{tot}(n)] \cdot s_{loc} \tag{10}$$

This means that a fraction s_{loc} of the specular energy is translated to diffuse energy.

When a receiver happens to be inside the pyramid being traced, it receives the specular intensity, which is computed as:

$$I_{spec} = \frac{W \cdot Q_{\vartheta}}{4 \cdot \pi \cdot (r_{1tot} + r_2)^2} \cdot \left[\prod_{i=1}^{N} (1 - \alpha_i) \right] \cdot (1 - s_{tot}) \tag{11}$$

in which W is the acoustic power of the source, with directivity Q_{ϑ}, r_{1tot} is the total path of the pyramid from the source to the last reflection point, r_2 is the distance between the

reflection point and the receiver, and α_i are the absorption coefficients of all the surfaces where the pyramid did reflect.

Instead, all the receivers which are in the positive hemispace in front of the surface where the reflection happened, also if they are not within the pyramid, receive the diffuse intensity, which seems to originate from a concentrated source located in the last reflection point, following the uniform scattering model (not Lambert):

$$I_{diff} = \frac{W \cdot Q_\vartheta \cdot \left[\prod_{i=1}^{N}(1-\alpha_i)\right] \cdot s_{tot}}{4 \cdot \pi \cdot {r_{1tot}}^2 + N_{pyr} \cdot 2 \cdot \pi \cdot {r_2}^2} \tag{12}$$

This equation is obtained redistributing the total power communicated by the pyramid to the elementary area A of the reflecting surface (see fig. 25) over a proper surface. The total incident power is:

$$W_{inc} = \frac{W \cdot Q_\vartheta}{N_{pyr}} \cdot \prod_{i=1}^{N}(1-\alpha_i) \tag{13}$$

After multiplying for the running scattering coefficient s_{tot}, it could appear reasonable to dilute this power, for computing the diffuse intensity, over the surface of a hemisphere of radius r_2. But this can cause intolerable artefacts if the receiver is very close to the reflection point, as this could make the diffuse intensity to become greater than the incident intensity:

$$I_{inc} = \frac{W \cdot Q_\vartheta}{4 \cdot \pi \cdot {r_{1tot}}^2} \cdot \prod_{i=1}^{N}(1-\alpha_i) \tag{14}$$

This explains the reason for which the first term was added in the denominator of eqn. 12, which substantially comes back to the dilution over an hemisphere when r_2 is very large, but reduces to the diffuse intensity on the surface as r_2 goes to zero.

After a long path r_{1tot} (in the late part of the reverberant tail), the value of s_{tot} is almost 1, and the pyramid base is so huge that all the receivers are always within it. So in practice the received intensity comes back to the same value, which was computed by the previous, diffuse-less version of the program.

This means that the introduction of the diffusion algorithms produces relevant modification only of the early part of the computed impulse response, as the first reflections, which previously resulted as isolated sharp peaks, are now followed by small diffuse tails, and this makes the simulation to look (and sound) much more realistic.

This means also that the original diffusion-less formulation of the Pyramid Tracing algorithm produced in practice a diffuse reverberant tail, but in that case the progressive transition between the first part of the echogram (deterministic and specular), and the second part (statistical and diffuse) was governed by the value of the critical time t_c:

$$t_C = \sqrt{\frac{{m_{fp}}^2 \cdot N_{pyr}}{4 \cdot c_0^2 \cdot \beta}} \tag{15}$$

As shown, t_c depends from the mean free path m_{fp} and from the adimensional shape factor β, which are invariant for a given geometrical case, but also from the number of pyramids N_{pyr}. This explains why, for each case, there was an "optimal" number of pyramids, and when this was exceeded, the simulation accuracy tended to reduce instead of improving. This effect was

clear by looking at the results of the PTB round robin on room acoustics simulation [17], where the pyramid tracing algorithm gave the best results with 2048 pyramids (and very little computation time, of course): attempting to improve the accuracy of the results by increasing the number of pyramids to 16384, the results became worst.

With the new formulation, the transition between the specular and diffuse behaviour is no more governed by the number of pyramids, because eq. 12 compensates for it. Instead, the transition depends on the rapidity with which the running scattering coefficient s_{tot} approaches 1, and this is affected by the values of the scattering coefficient of the surfaces hit, but also on the number of edges included in the geometry under test.

9. Comparison with experimental results

A simple comparison with the experimental results, already employed for the measurement of the scattering and diffusion coefficients, will be presented here.

Fig. 26 shows the geometrical CAD model of the case under test, which closely correspond to the laboratory setup described in this paper: a loudspeaker is mounted flush in the floor (so that we can disregard completely the presence of the floor itself), and a diffusing panel is suspended above it. 255 microphone positions are considered, along a straight line passing horizontally, midway between the loudspeaker and the panel, and an highly-detailed impulse response is computed at each receiver (time resolution is approximately 0.06 ms).

Four cases were modelled: a flat, polished panel (scattering coefficient was zero, only edge effects), an highly diffusing flat panel (a Schroeder-type diffuser) and a curved, polished surface rotated both along the direction of maximum diffusion and of minimum diffusion, which was also modelled as a flat panel with proper values of the absorption and scattering coefficients.

The experimental results of the same four cases were presented in par. 5 (fig. 9,10). Figgs. 27, 28, 29, and 30 show the results of the numerical simulations obtained with Ramsete-II (pyramid tracing with diffusion) at 1 kHz. For checking the similitude of the numerical and experimental results in a quantitative way, a sort of "pattern-matching" between the images was attempted. In practice, each image is a matrix, having 255 rows and 400 lines (26 ms), and each cell contains a sound intensity (in W/m^2). So it is possible to compute an RMS relative error, and express it in dB, with the following expression:

$$E = 10 \cdot \lg \left[\sqrt{\frac{\sum_{i=1}^{N} \left(I_{sper,i} - I_{num,i} \right)^2}{\sum_{i=1}^{N} \left(I_{sper,i} \right)^2}} \right] \qquad (16)$$

This value is an indicator of the simulation's error in comparison with the experimental result, and can be assimilated to a sort of a Noise-to-Signal ratio.

Each simulation was repeated 3 times, with different values of the scattering coefficient: in the first case it was assumed to be zero (no surface scattering), in the second case it was set equal to the scattering coefficient s, derived in par. 7 from the experimental results, and in the third case it was set equal to the AES diffusion coefficient d, defined in [1,2] and also computed from the experimental results as reported in par. 6. The following table presents the obtained results, in terms of the average error E:

Input parameters (absorption, scattering and diffusion coefficients) and results of the percentage error, in dB, between numerical and experimental results

Parameter	Flat Panel	Galav2 diffuser	curved panel	curved panel (90°)
α	0	0.03	0.286	0.76
S	0.117	0.86	1	0.20
D	0.35	0.86	0.92	0.52
E_0	-4.12	+3.45	+1.70	-3.99
E_s	**-4.28**	**-4.75**	**-6.42**	**-4.71**
E_d	-3.73	-4.75	-5.21	-4.33

Ranking the results, it can be concluded that the best results are obtained, as expected, when the correct value of the scattering coefficient is employed. Nevertheless, the use of the diffusion coefficient in its place increases the error, but this always remains much lower than neglecting completely the scattering effect by inserting a zero value.

Looking at fig. 29, anyway, it is evident that modelling a curved diffuser as a flat surface produces a simulated sound field very different from the experimental one. This is due to the fact that a diffuse tail is produced, whilst in practice the reflected sound is always a sharp peak. Repeating the simulation, but having actually designed the true shape of the surface, assigning to it a diffusion coefficient = 0, and switching off the edge diffusion computation, produces a more realistic simulation of a curved surface, as it is clearly shown in fig. 31.

10. Conclusions

In this paper a new measurement technique, based on the Wave Field Synthesis method, is described. Through this technique, it is possible to derive the values of the two recently defined descriptors of the scattering behaviour of a surface: the ISO scattering coefficient and the AES diffusion coefficient. The measurement is robust and requires little effort.

The extension of a numerical simulation program, based on the pyramid tracing approach, was also described: with minimal computation overhead, now the algorithm takes properly into account the scattering from rough surfaces and from the edge of each panel.

From the comparison of the numerical results with the experimental data, it resulted that the values of the AES diffusion (uniformity) coefficient are not always satisfying for the numerical computations made under the hypothesis of geometrical acoustics: the experimental results are better approximated making use of the ISO scattering coefficient, which can differ significantly from the diffusion (uniformity) coefficient.

The experimental apparatus developed for this research made it possible to employ some parts of the Wave Field Synthesis theory: this revealed particularly useful for obtaining a graphical representation of the scattered wavefronts, but also for the separation of the direct and reflected waves. In principle, with similar techniques it could be possible to separate the diffuse from the specular reflections, and this remains a topic on which further research is required.

11. Acknowledgements

This work was supported by a research convention with Audio Link – Alberi (Parma), Italy and from the Italian Ministry for University and Research (MURST) under the grant MURST-98 #9809323883 (which was co-funded by ASK Automotive Industries, Reggio Emilia, Italy).

The substantial contribution of Michele Zanolin and Elisa Crema to the experimental measurements was highly appreciated, along with the effort spent by Paolo Galaverna and Guido Truffelli for the development of the required software routines.

12. References

[1] T.J. Hargreaves, T.J. Cox, Y.W. Lam, P. D'Antonio, "Characterising scattering from room surfaces", proc. 16th ICA and 135th Meeting A.S.A., Seattle WA, vol. IV, pp. 2731-2732, June 1998.

[2] P. D' Antonio, T. Cox, "Two Decades of Sound Diffusor Design and Development, Part 2: Prediction, Measurement and Characterization" Journal of AES vol. 46, n° 12, pp. 1075-1091 (December 1998).

[3] E. Mommertz, M. Vorlander, "Measurement of scattering coefficients of surfaces in the reverberation chamber and in the free field" – Proc. 15th Internat. Congress on Acoustics, Trondheim, 1995, pp. 577-590.

[4] A. J. Berkhout, P. Vogel, D. de Vries, "Use of Wave Field Synthesis for Natural Reinforced Sound" – Pre-prints of the 92th AES Convention, #3299, March 1992

[5] D. de Vries, A. J. Berkhout, J. J. Sonke, "Array Technology for Measurement and Analysis of Sound Fields in Enclosures" - Pre-prints of the 101th AES Convention, #4266, May 1996.

[6] Diemer de Vries and Jan Baan, "Auralization of Sound Fields by Wave Field Synthesis" - Pre-prints of the 106th Convention, Munich, Germany, 1999 May 8–11, # 4927.

[7] Naylor G.M. - "ODEON - Another Hybrid Room Acoustical Model" - Applied Acoustics Vol. 38 no.s 2-4, pag. 131 (1993).

[8] B.I. Dalenbäck, "Verification of Prediction Based on Randomized Tail-Corrected Cone-Tracing and Array Modeling", 137th ASA/2nd EAA Berlin (March 1999).

[9] A. Farina, F. Righini, "Software implementation of an MLS analyzer, with tools for convolution, auralization and inverse filtering", Pre-prints of the 103rd AES Convention, New York, 26-29 September 1997.

[10] O. Kirkeby and P. A. Nelson – "Digital Filter Design for Virtual Source Imaging Systems", Pre-prints of the 104th AES Convention, Amsterdam, 15 - 20 May, 1998.

[11] A. Farina, "Simultaneous measurement of impulse response and distortion with a swept-sine technique", Pre-prints of the 108th AES Convention, Paris, 19-22 February 2000.

[12] A.Farina, "Measurement of the surface scattering coefficient: comparison of the Mommertz/Vorlander approach with the new Wave Field Synthesis method" - International Symposium on Surface Diffusion in Room Acoustics, Liverpool, 16/4/2000 – downloadable from HTTP://pcfarina.eng.unipr.it .

[13] A. Farina, A. Torelli - "Measurement of the sound absorption coefficient of materials with a new sound intensity technique" - Pre-prints of the 102nd AES Conference, Berlin, 23-26 March 1997.

[14] A. Farina - "RAMSETE - a new Pyramid Tracer for medium and large scale acoustic problems" - Euro-Noise 95 Conference, Lyon 21-23 march 1995.

[15] A. Farina - "Pyramid Tracing vs. Ray Tracing for the simulation of sound propagation in large rooms" - In the volume "Computational Acoustics and its Environmental Applications", pp. 109-116, Editor C.A. Brebbia, Computational Mechanics Publications, Southampton (GB) 1995.

[16] A. Farina - "Verification of the accuracy of the Pyramid Tracing algorithm by comparison with experimental measurements by objective parameters" - ICA95 (International Conference on Acoustics), Trondheim (Norway) 26-30 June 1995.

[17] I. Bork, "A comparison of Room Simulation Software - The 2nd Round Robin on Room Acoustical Computer Simulation" – Acustica - Acta Acustica – Special Issue on Room Acoustics, vol. 6, n. 86, December 2000.

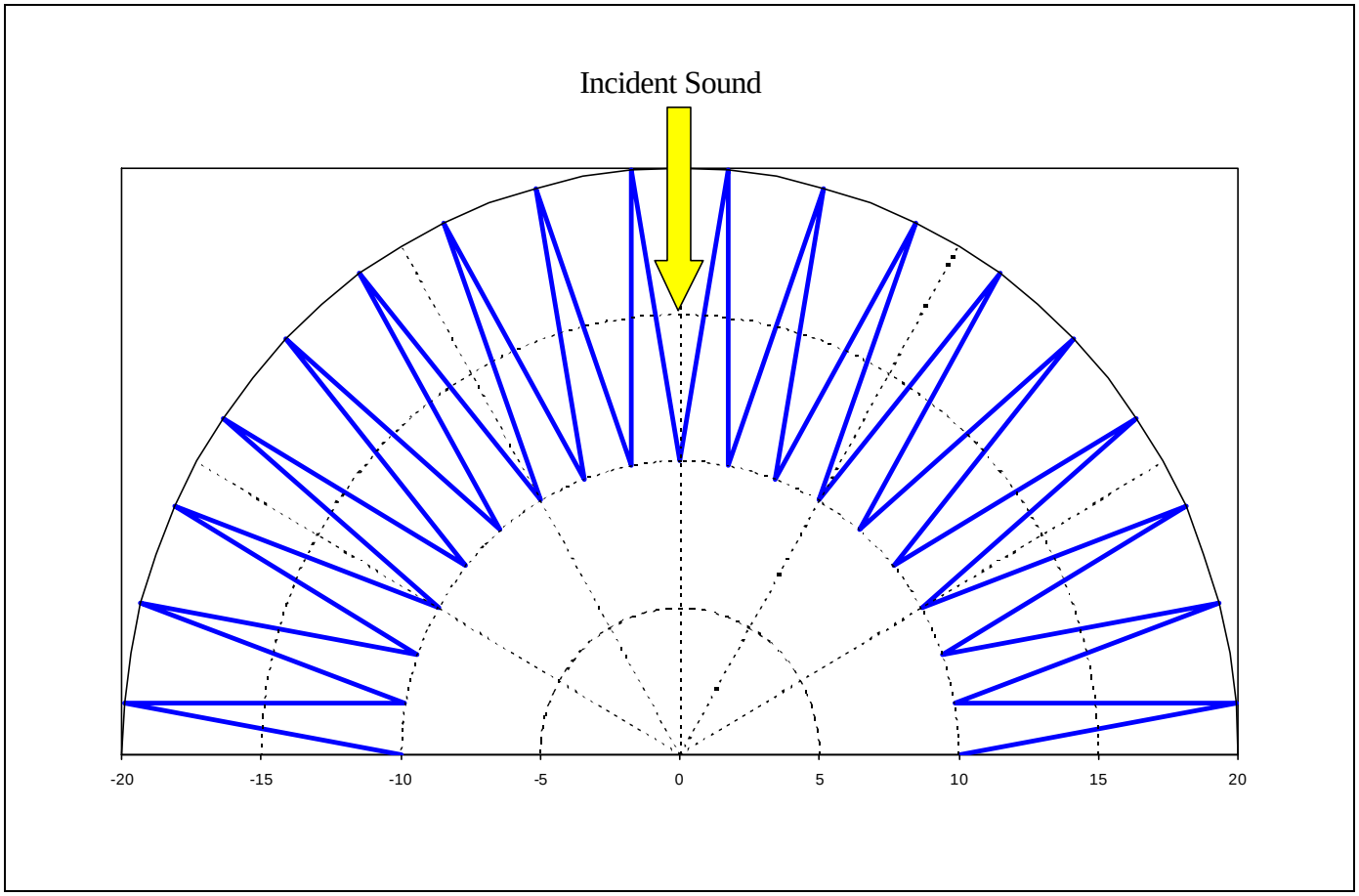

Fig. 1 - Saw-tooth polar reflection pattern with no specular reflection

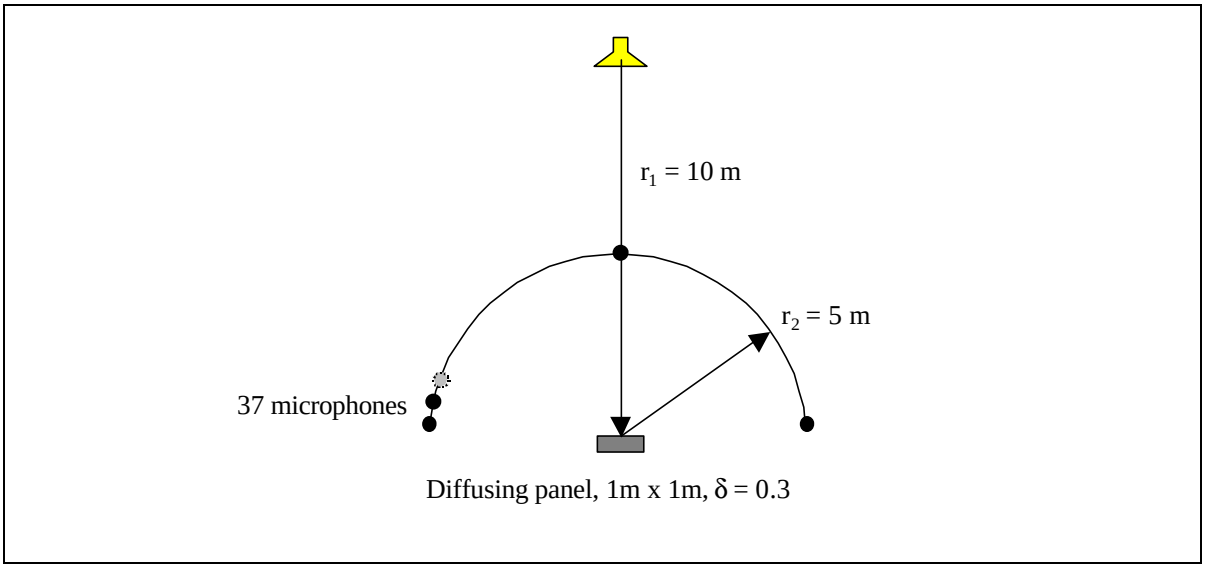

Fig. 2 – geometry of the theoretical case for comparison between the diffusion coefficients

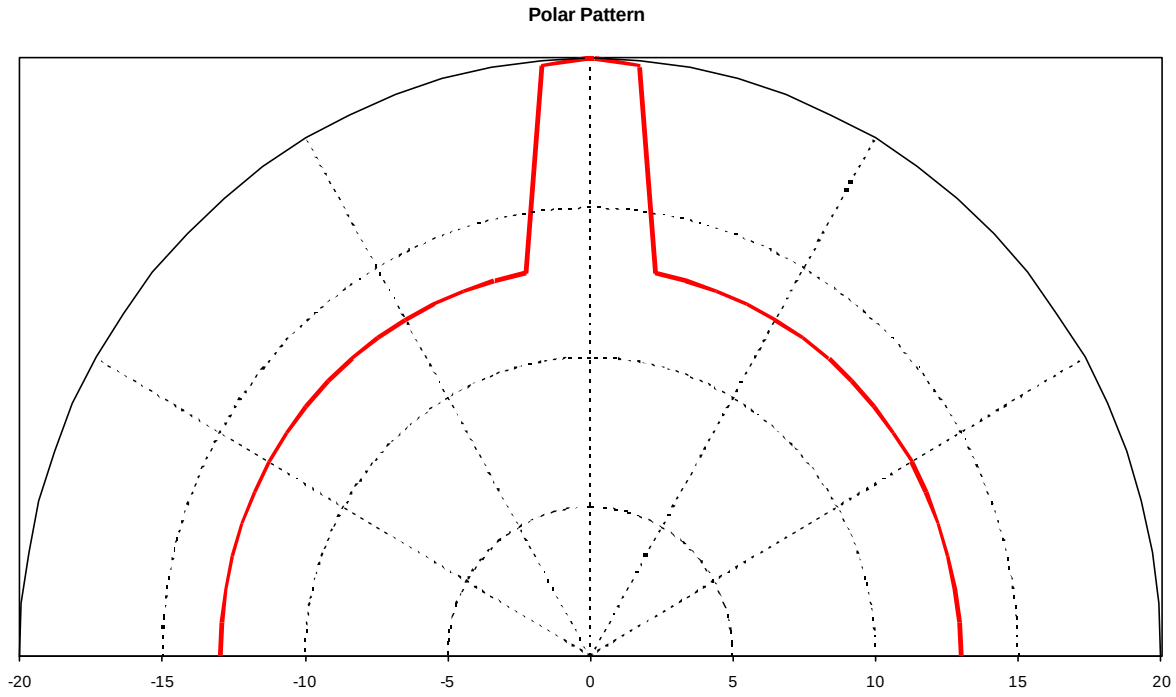

Fig. 3 - Theoretical polar pattern of the intensity reflected by a 1m•1m panel with δ=0.3

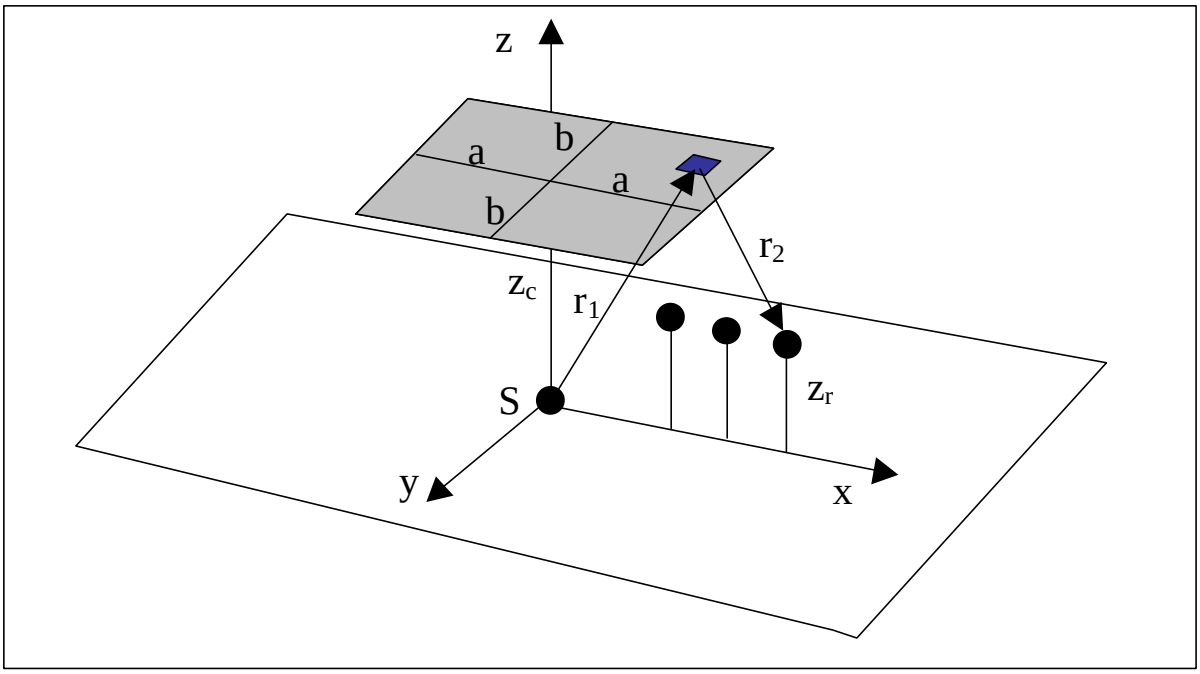

Fig. 4 – Schematic geometry of the experimental apparatus

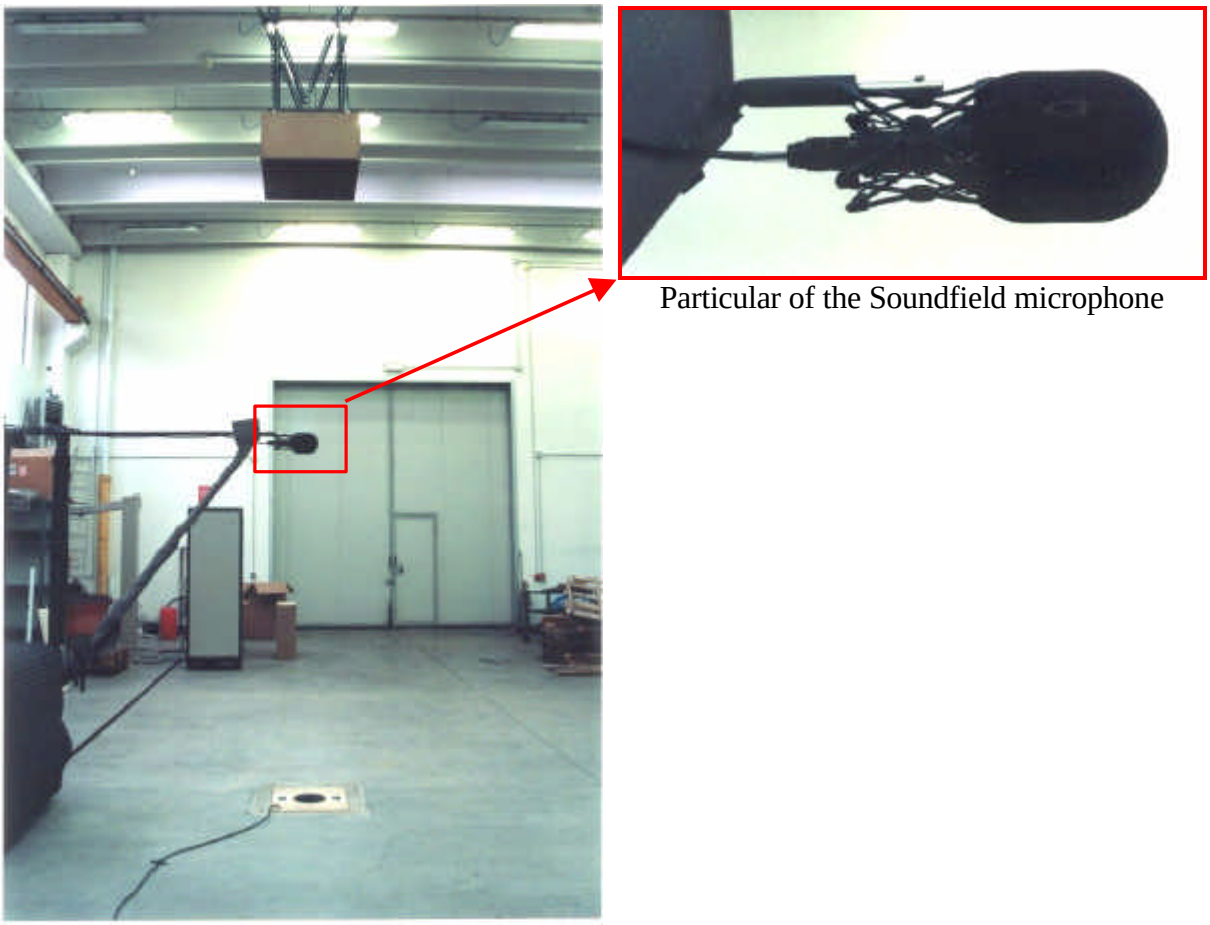

Fig. 5 – Experimental apparatus – Overall view

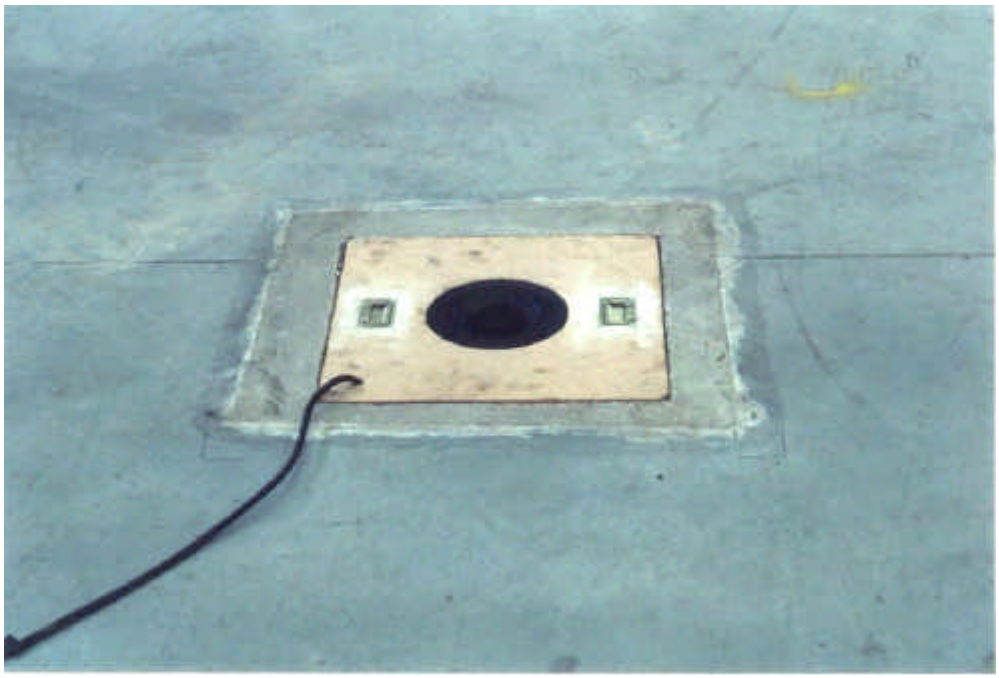

Fig. 6 – Particular of the loudspeaker inserted in the floor

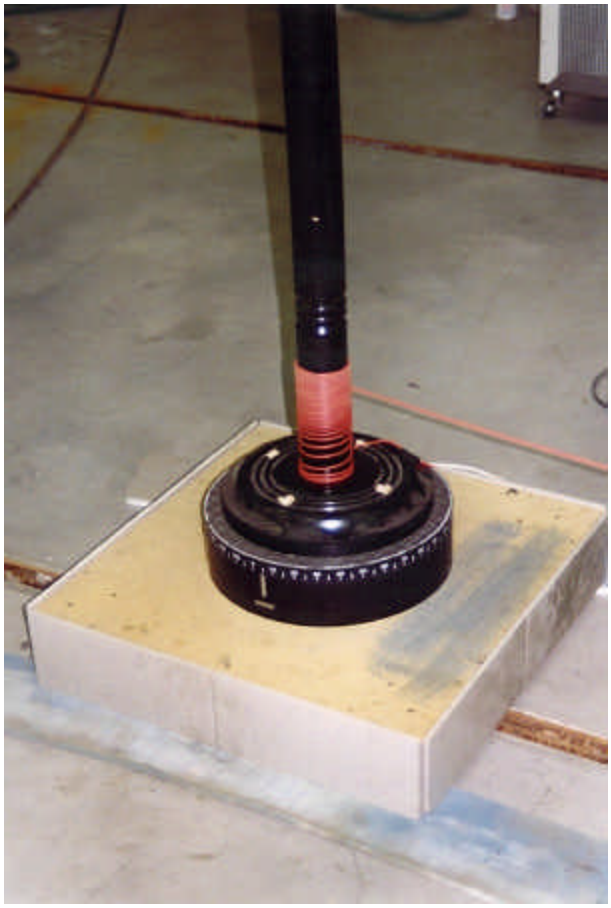

Fig. 7 –Particular of the rotating board with the cable folding around the drum.

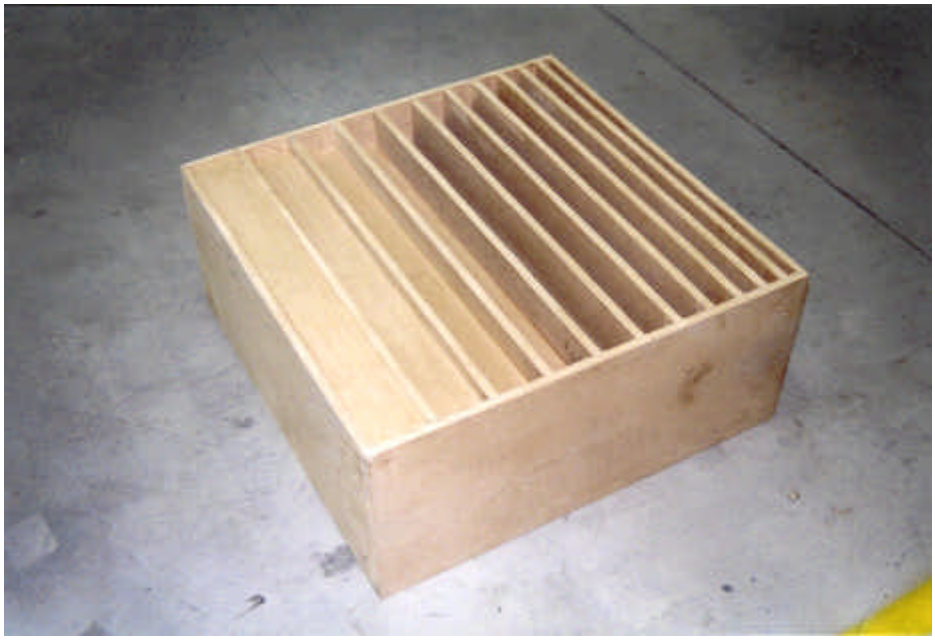

Fig. 8 – the diffusing panel (named GALAV2) on the reflecting floor.

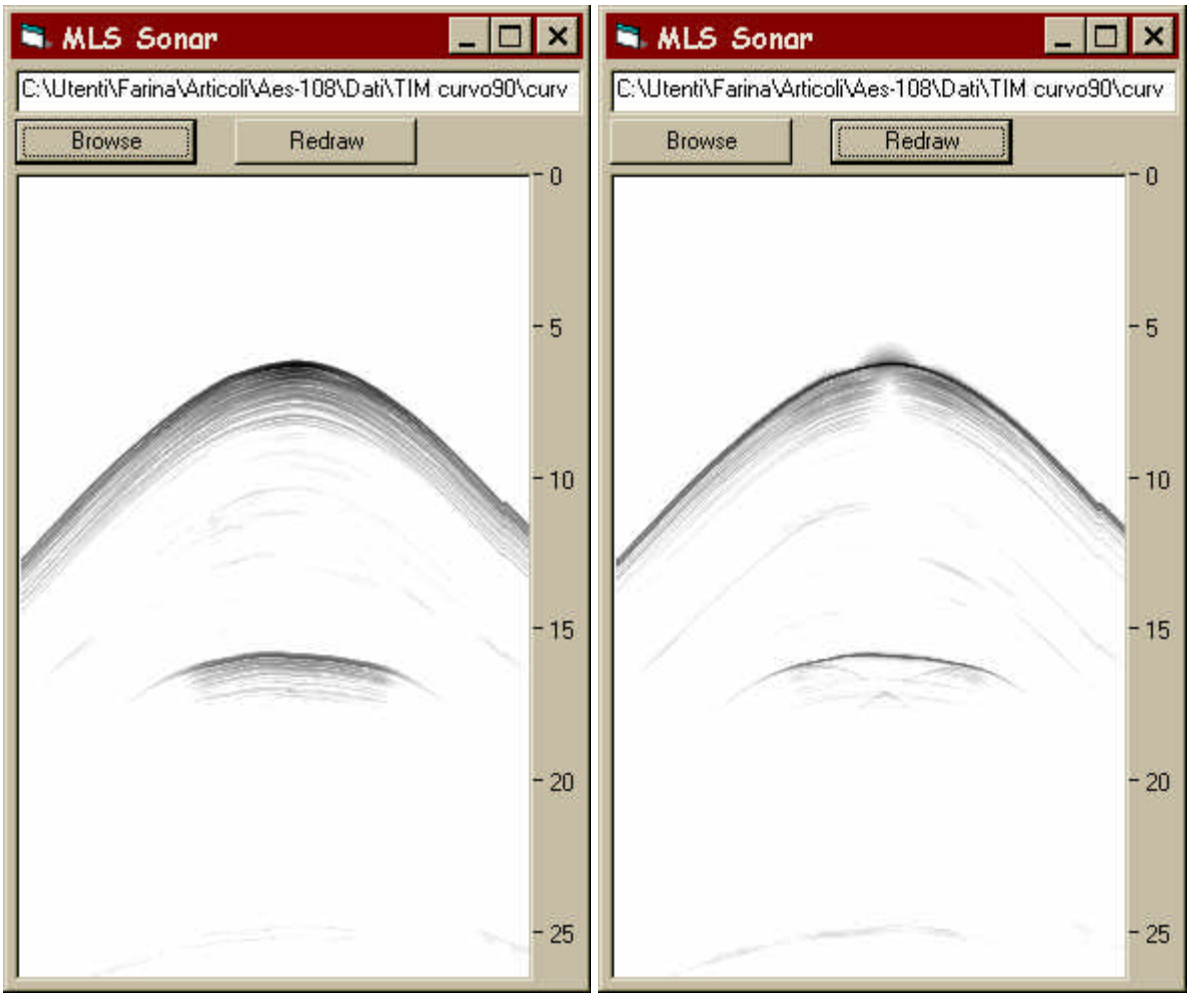

Fig. 9 – Measurement on the curved panel, along its axis, original (left) and after convolution with the Kirkeby inverse filter (right)

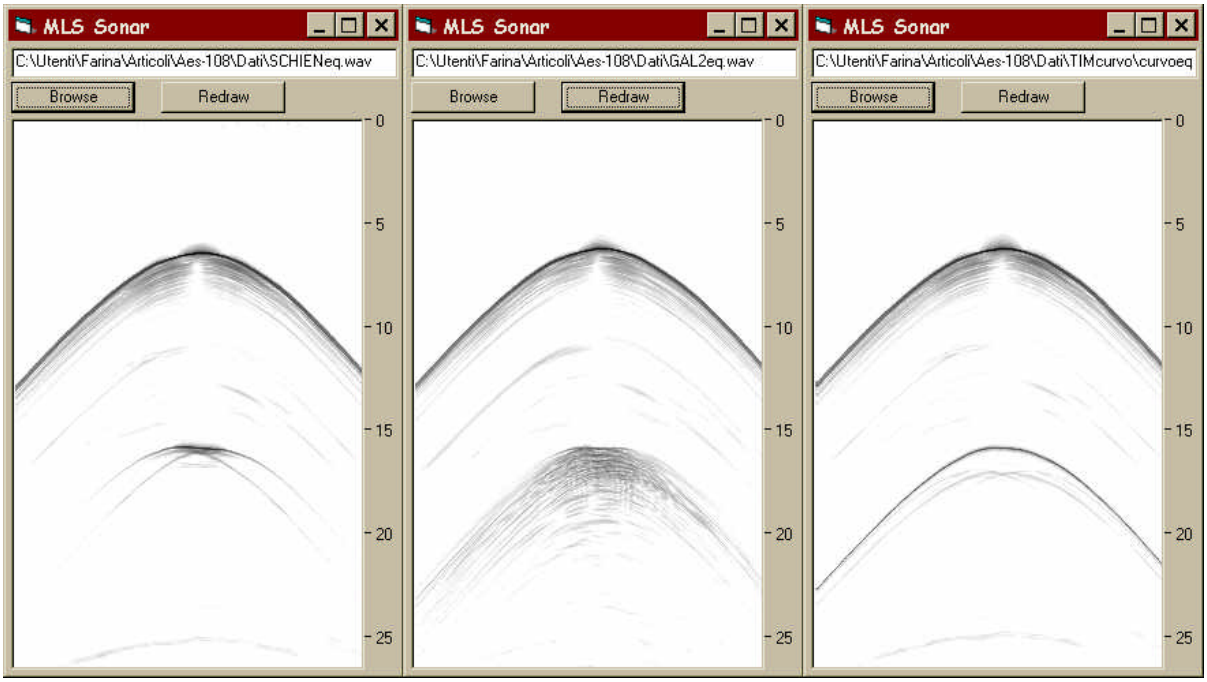

Fig. 10 – responses of three different panels

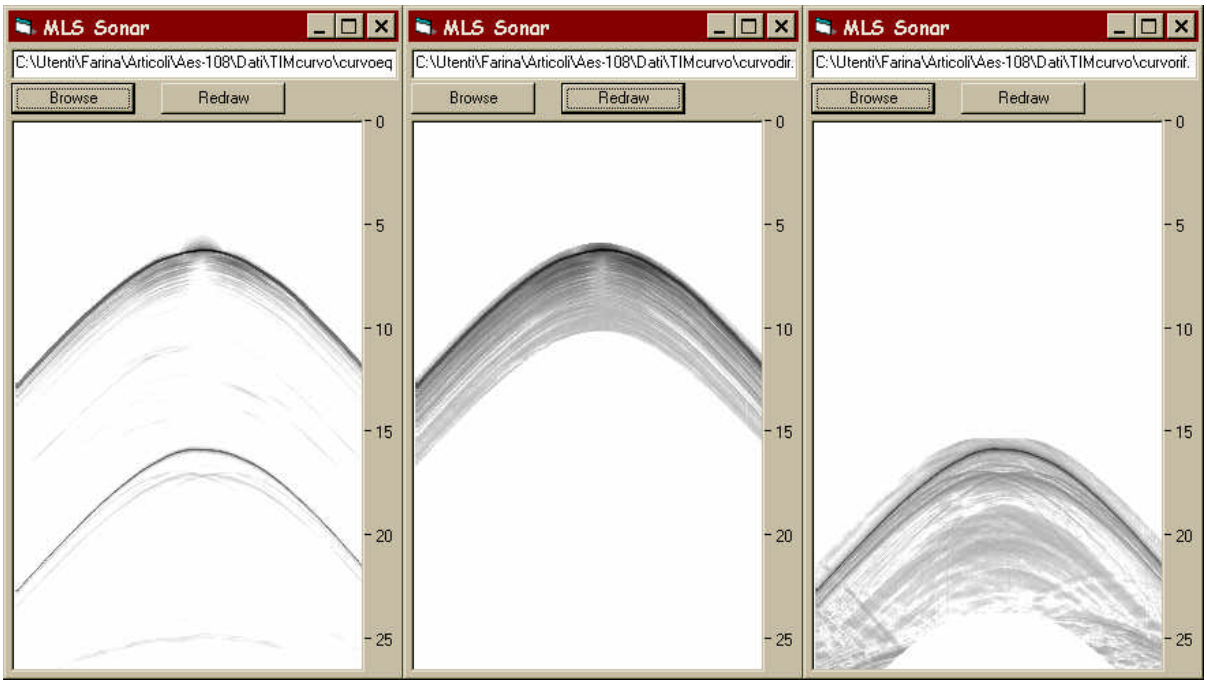

Fig. 11 – windowing of the original signal (left) in the direct (center) and reflected (right) components

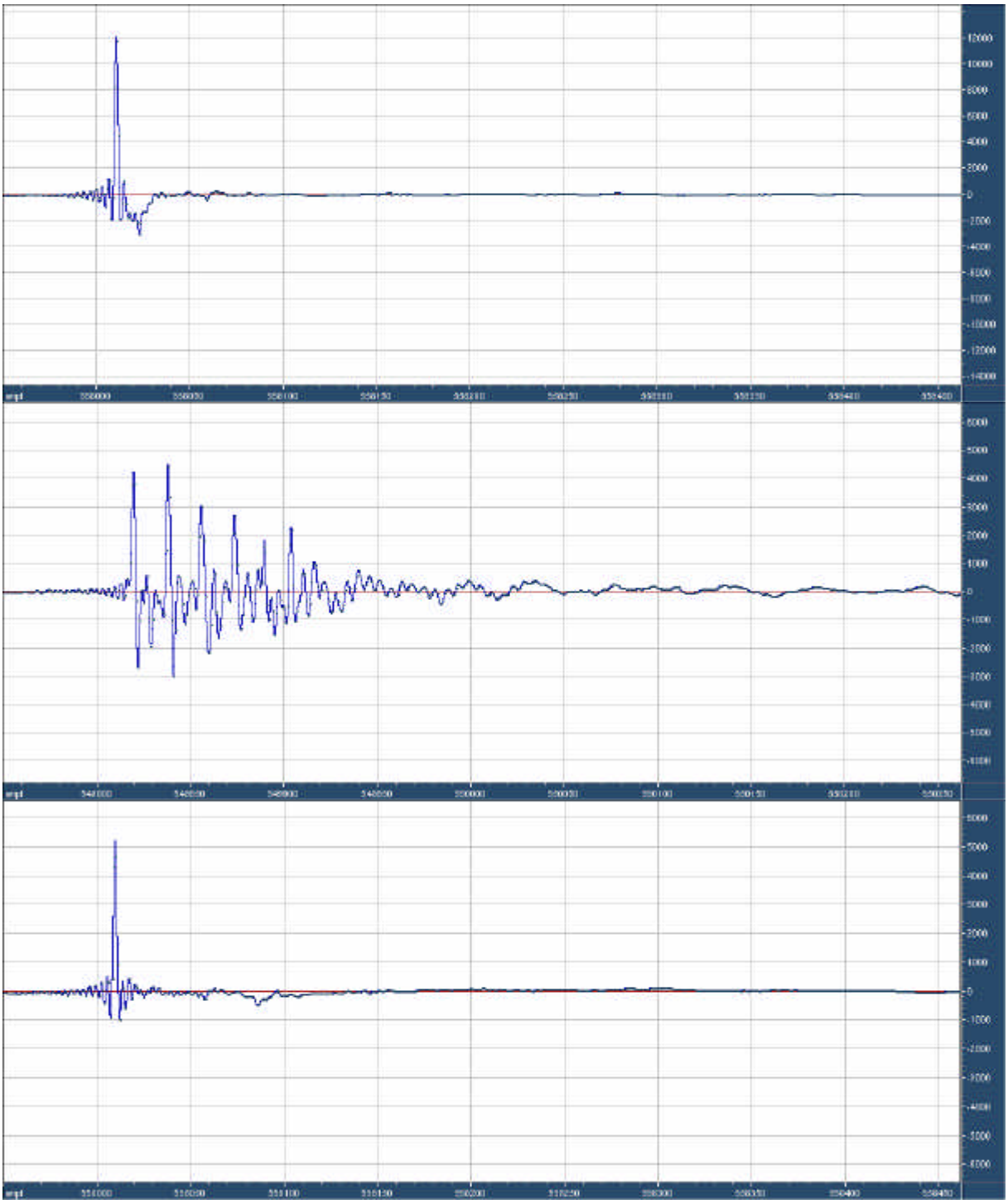

Fig. 12 – Waveform of the reflected signals – Flat panel (above),
diffusing panel (middle), curved panel (below)

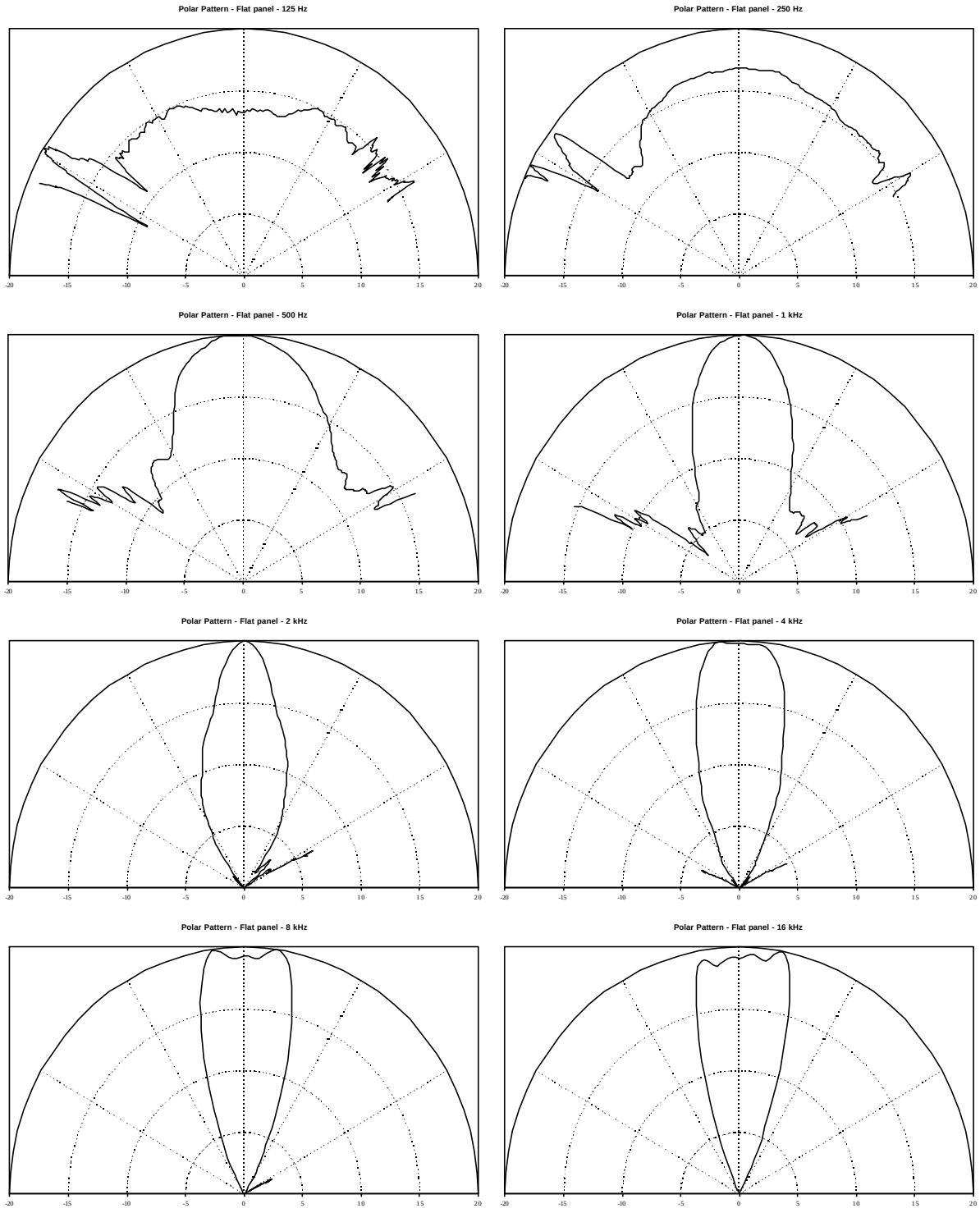

Fig. 13 – Polar patterns of the flat panel

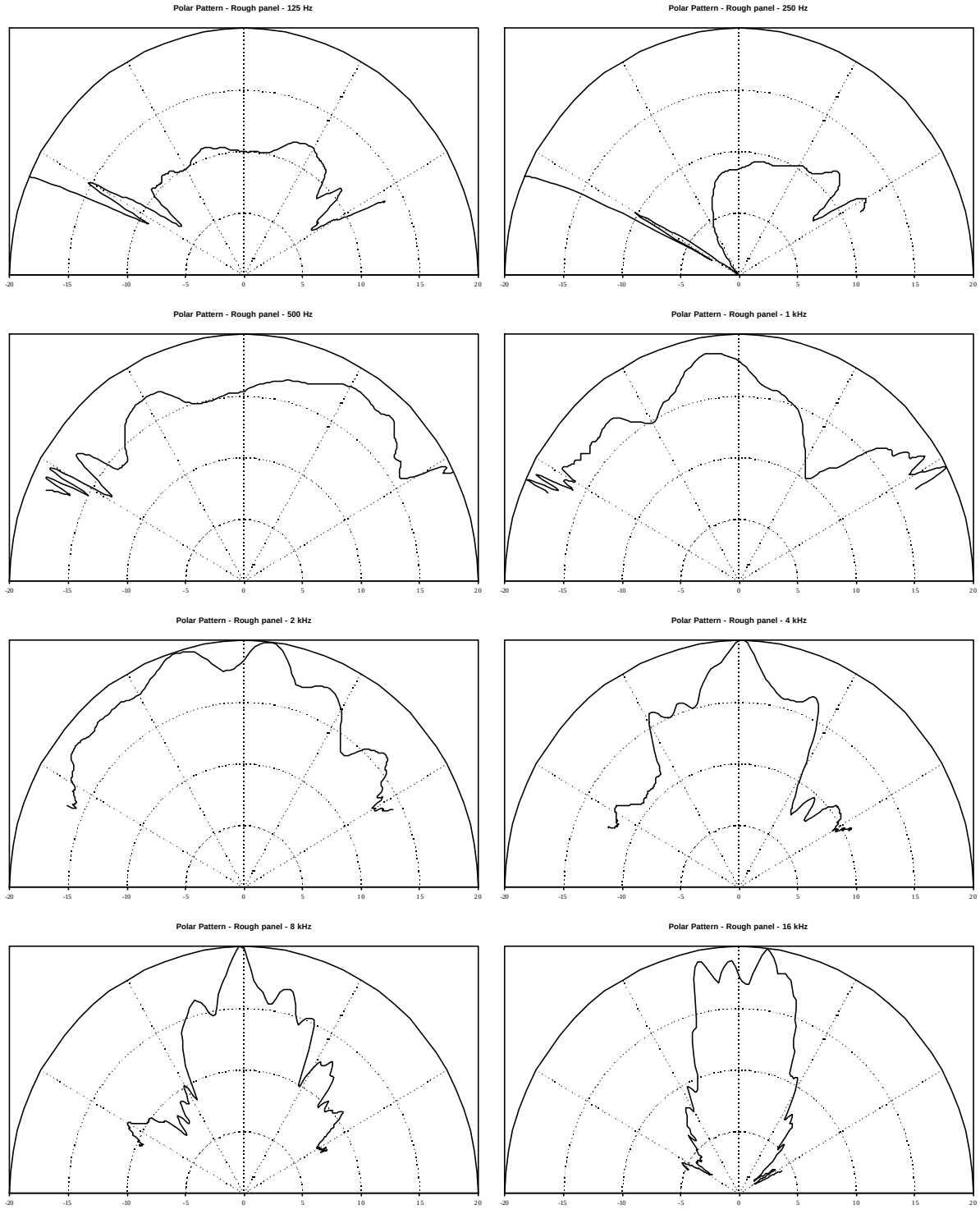

Fig. 14 – Polar patterns of the GALAV2 diffusing panel

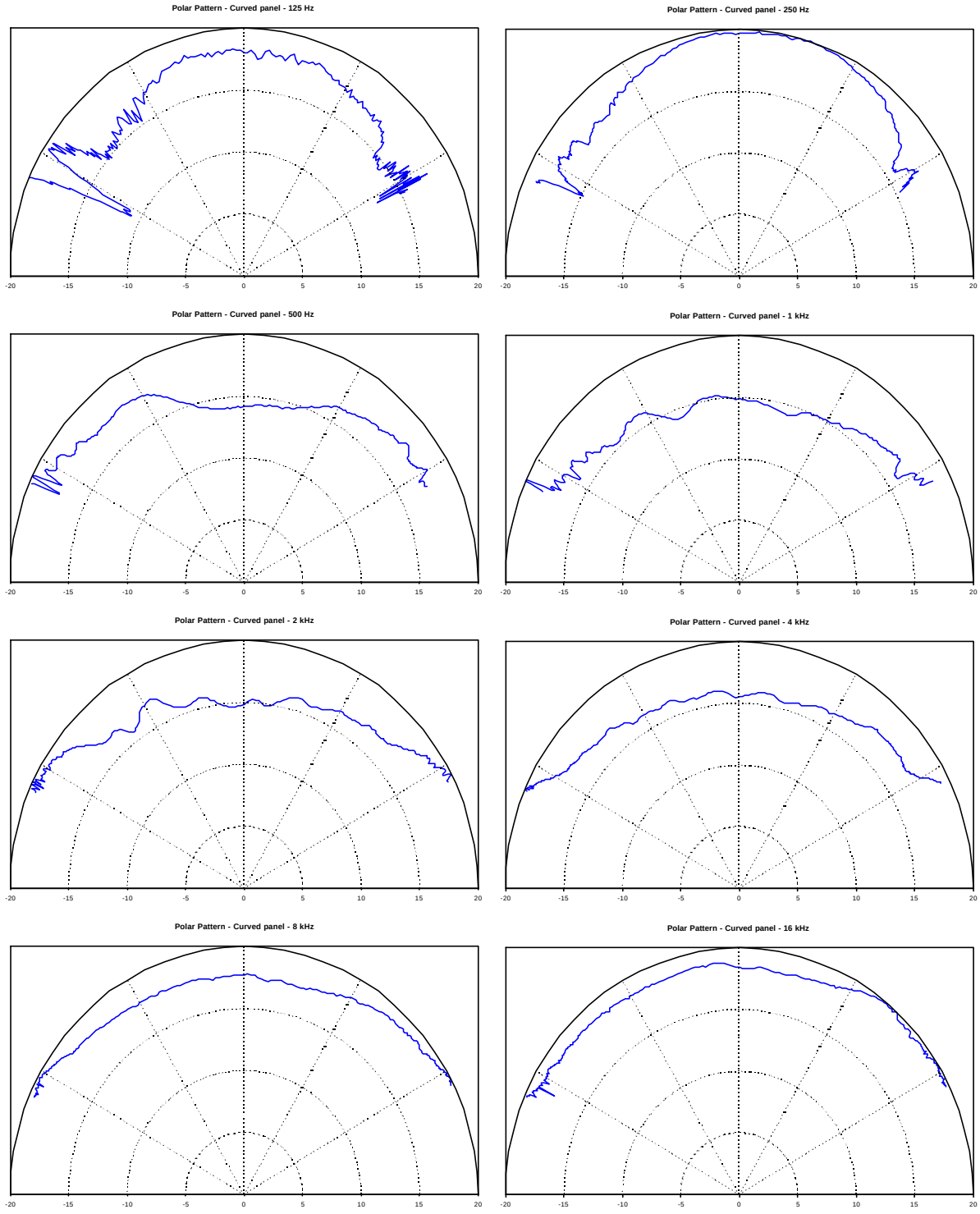

Fig. 15 – Polar patterns of the curved panel, maximum diffusion direction

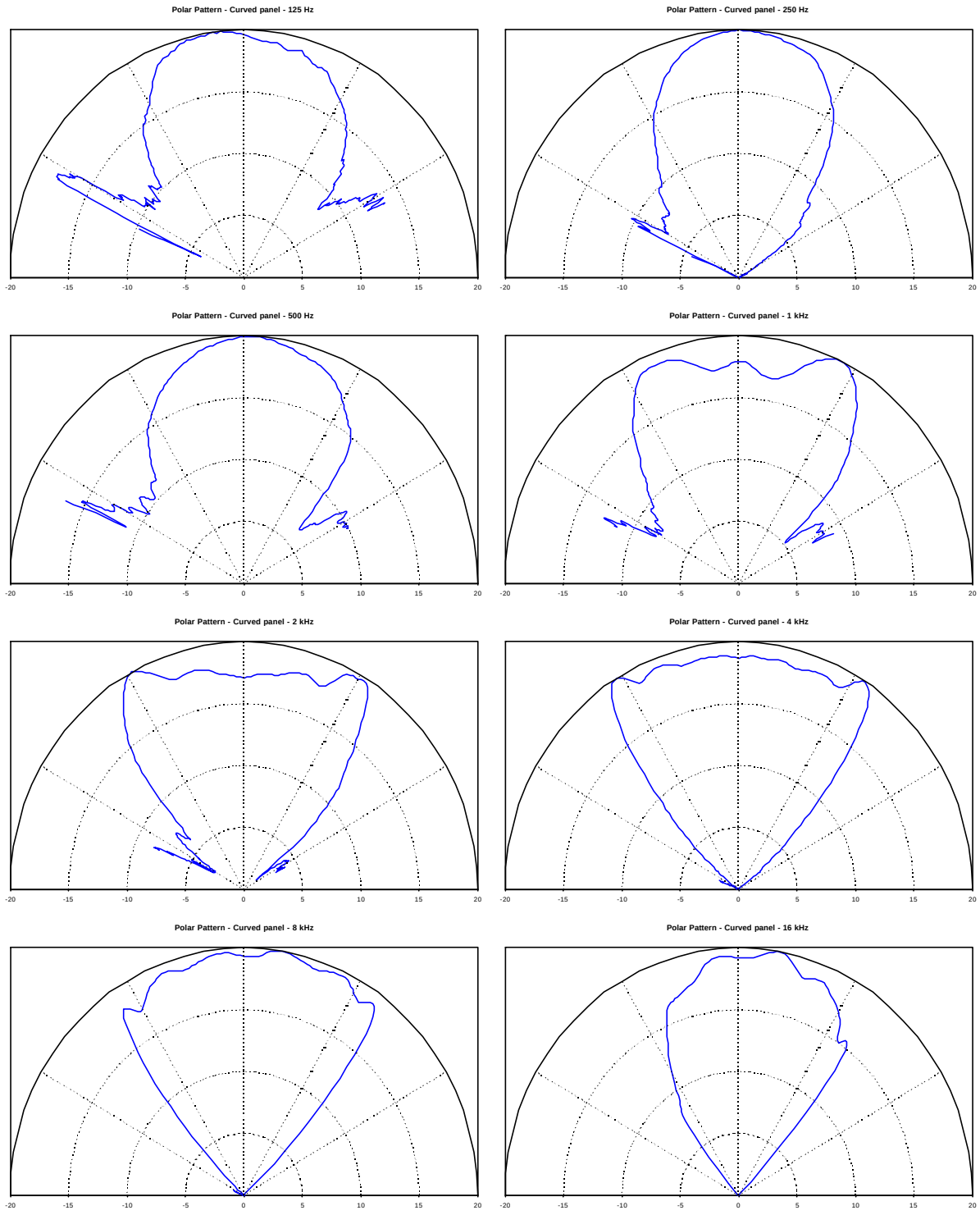

Fig. 16 – Polar patterns of the curved panel – rotated by 90° (minimum diffusion)

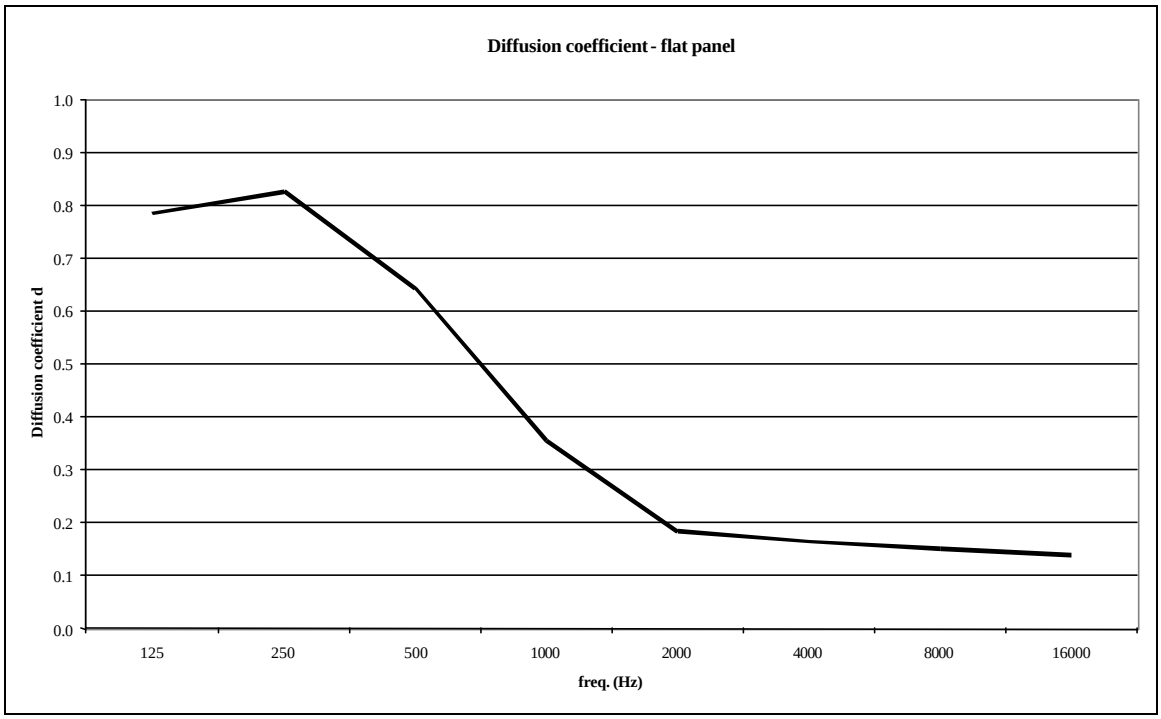

Fig. 17 – Values of d for the flat panel

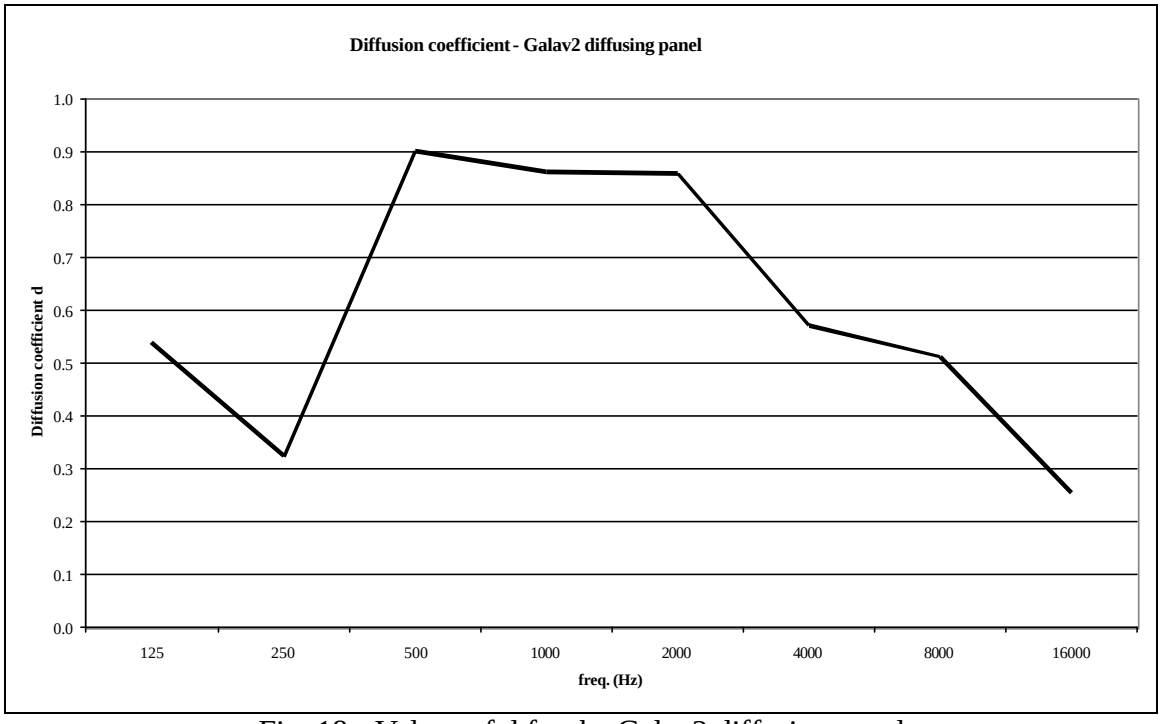

Fig. 18 - Values of d for the Galav2 diffusing panel

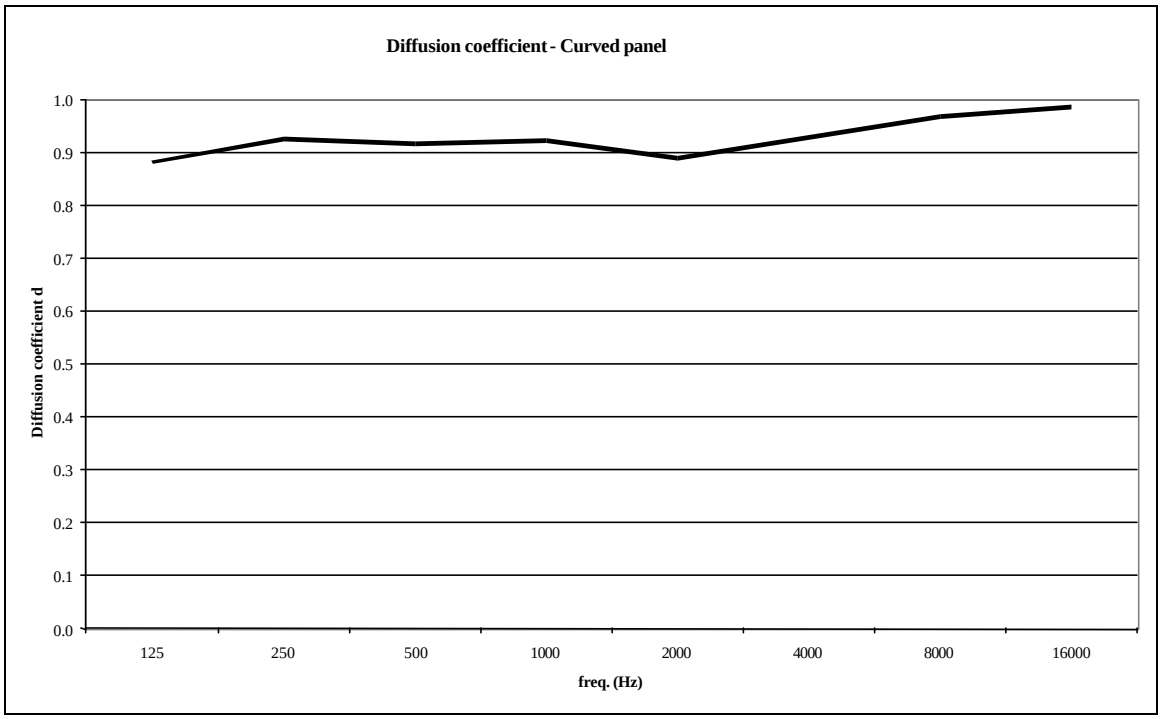

Fig. 19 - Values of d for the curved panel – maximum diffusion direction

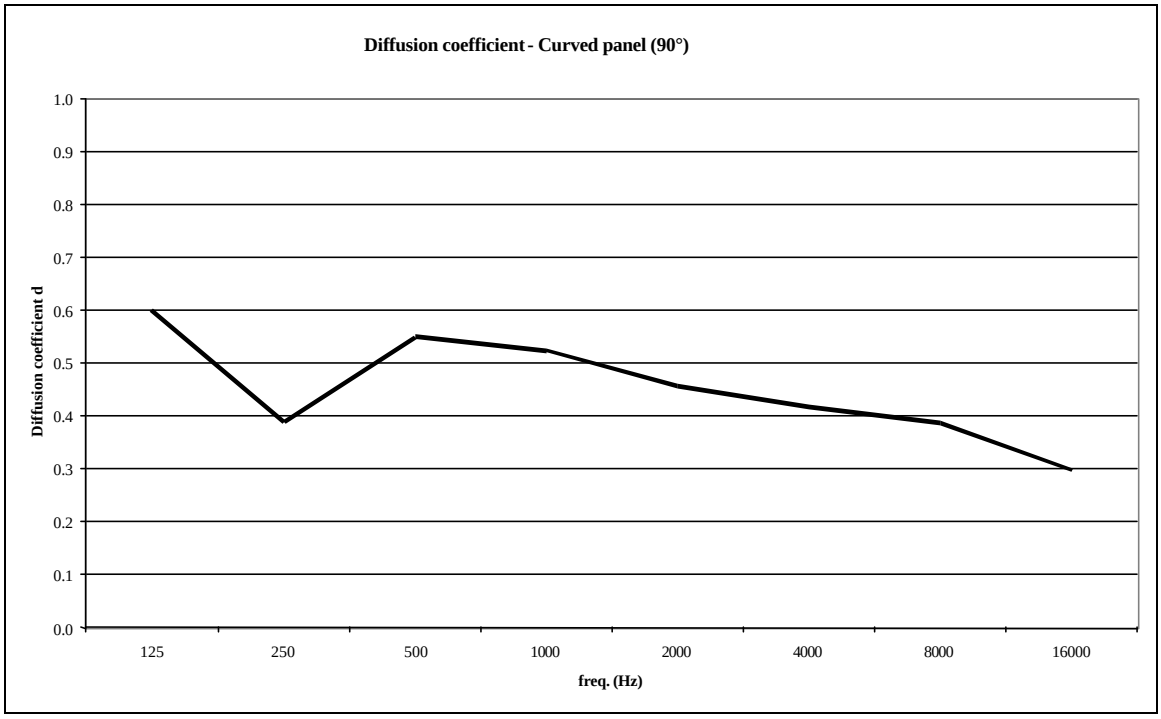

Fig. 20 - Values of d for the curved panel – minimum diffusion direction

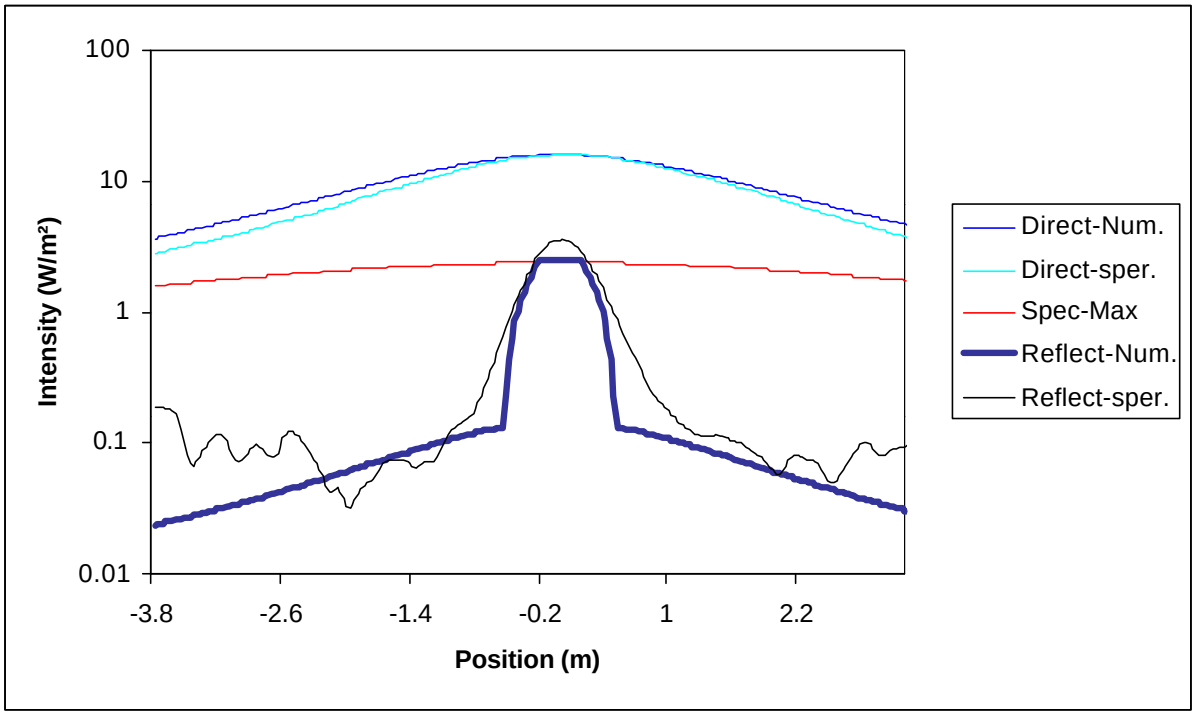

Fig. 21 – matching between numerical and experimental data – Flat Panel

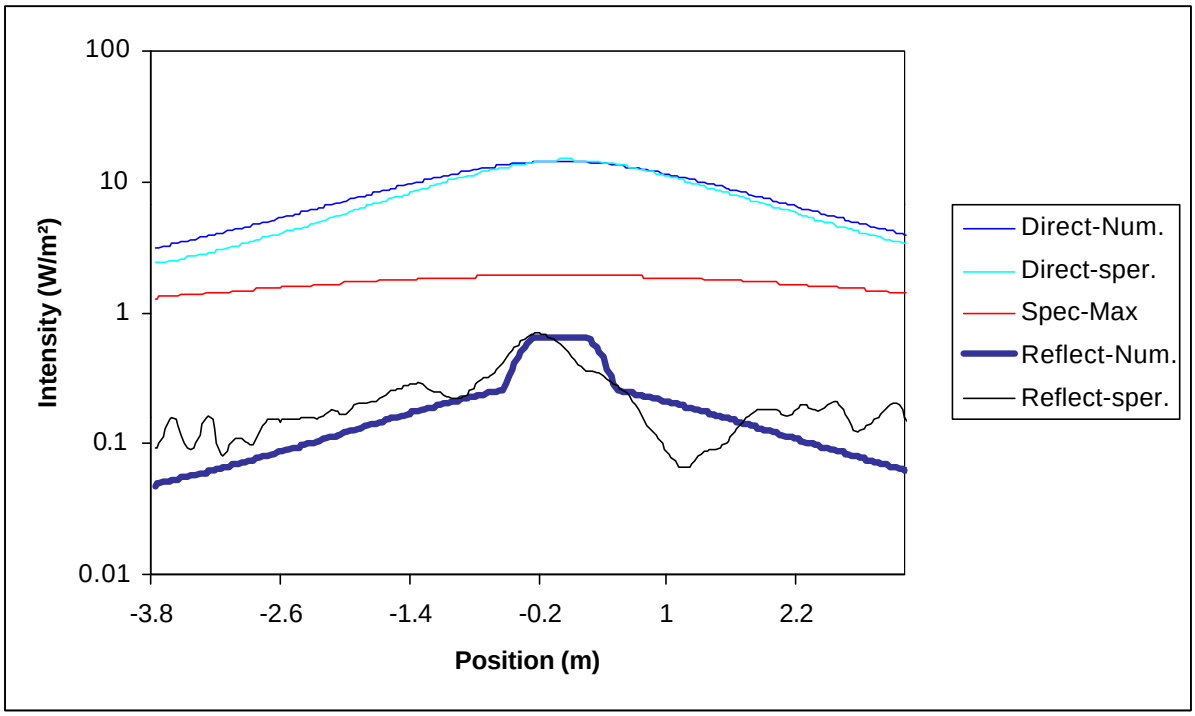

Fig. 22 – matching between numerical and experimental data – Galav2 diffusor

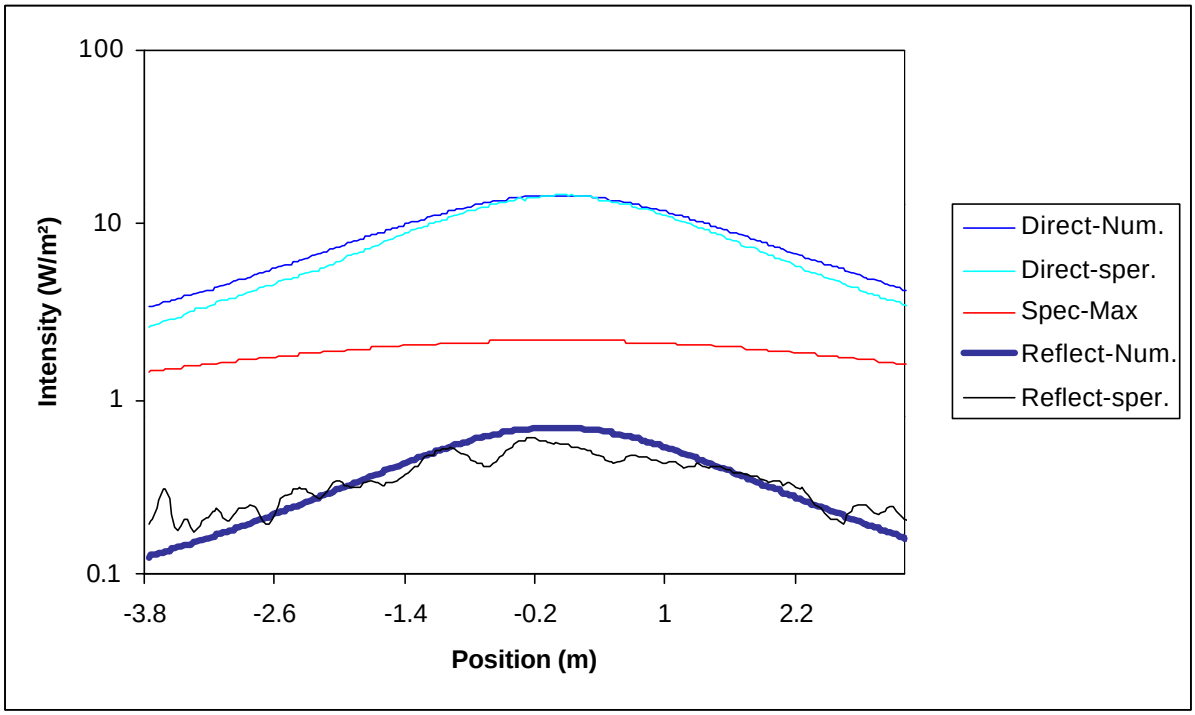

Fig. 23 – matching between numerical and experimental data – Curved Panel

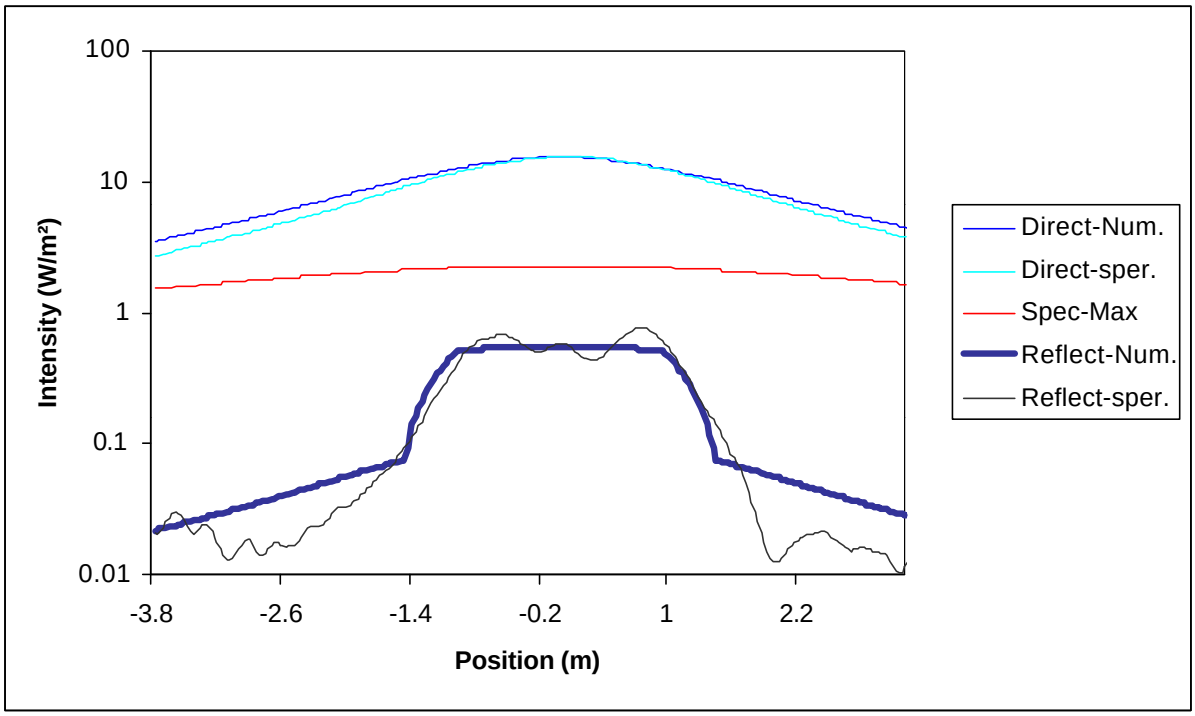

Fig. 24 – matching between numerical and experimental data – Curved Panel at 90°

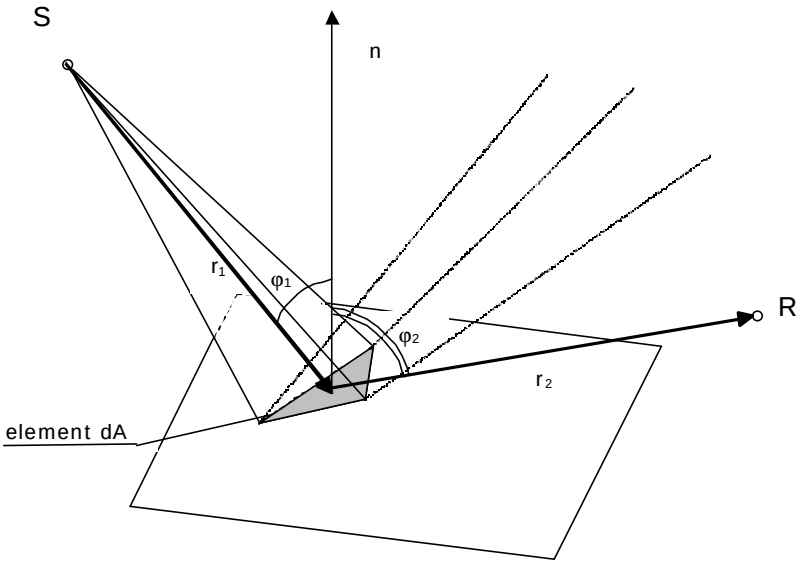

Fig. 25 – a pyramid impacting over a reflecting surface

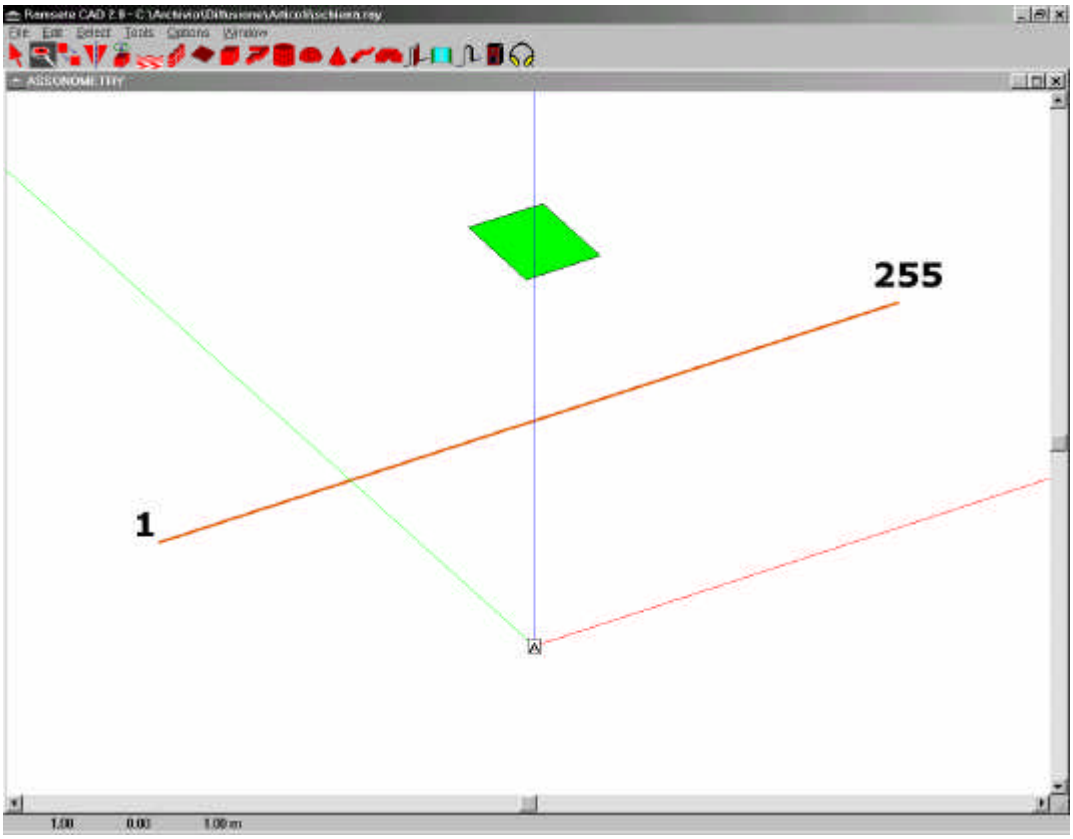

Fig. 26 – CAD representation of the measurement setup

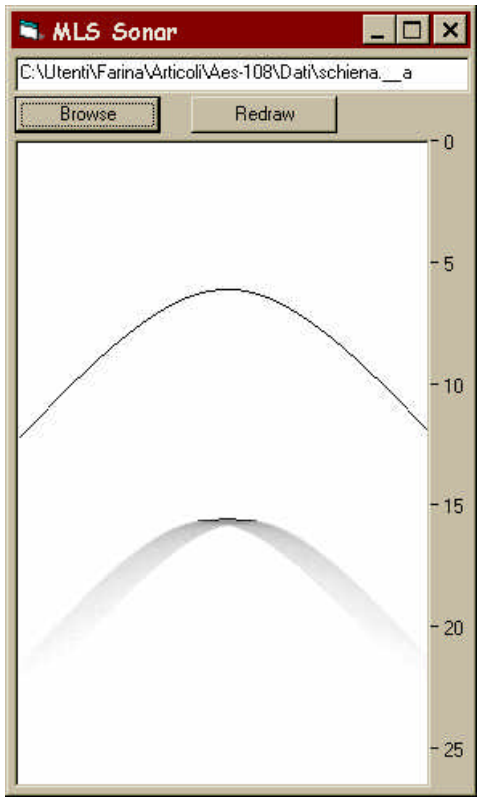

Fig. 27 – numerical simulation of the diffusion from a flat, square panel (s=0.117)

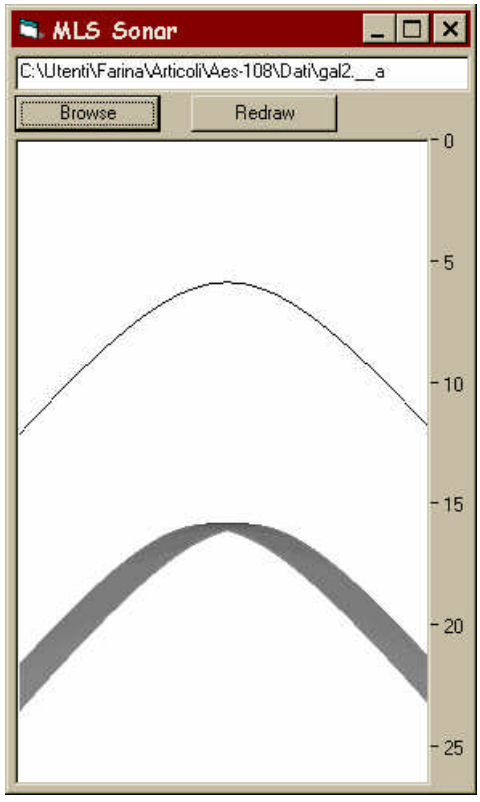

Fig. 28 – numerical simulation of the diffusion from a square diffuser (s=0.86)

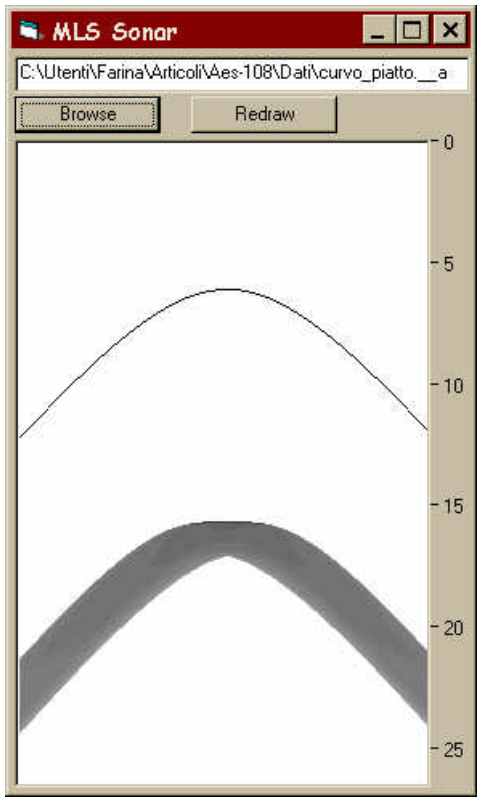

Fig. 29 – numerical simulation of the diffusion from a curved surface, along the direction of maximum diffusion, modeled as a flat panel with high diffusion coefficient (s=1)

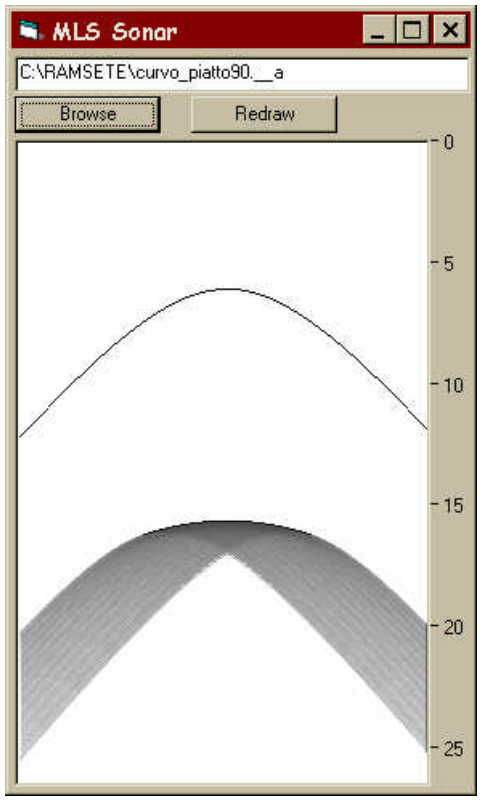

Fig. 30 – numerical simulation of the diffusion from a curved surface, along the direction of minimum diffusion, modeled as a flat panel with low diffusion coefficient (s=0.2)

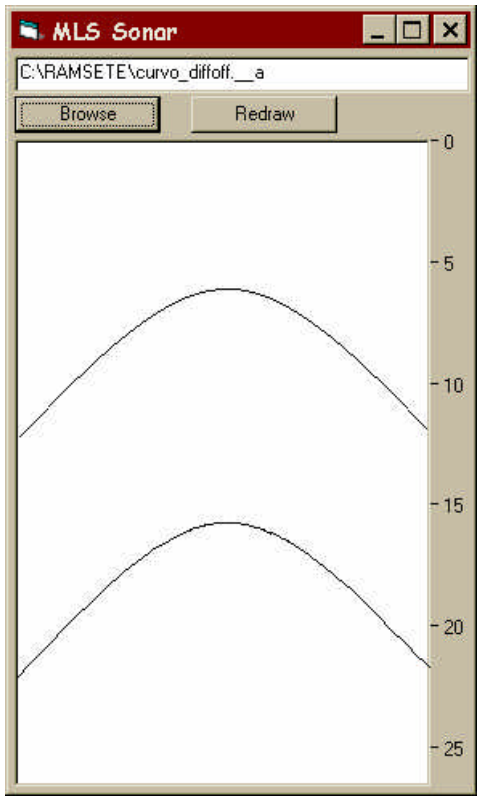

Fig. 31 - numerical simulation of the diffusion from a curved surface, modelled as a curved panel without diffusion coefficient (s=0)